Petroleum Science 22 (2025) 1653–1669

Contents lists available at ScienceDirect

Petroleum Science

journal homepage: www.keaipublishing.com/en/journals/petroleum-science

Original Paper

Mechanical differences of laminations and crack propagation mechanism of continental shale

Yong-Ting Duan [a, b, *], Cheng-Cheng Zhu [a, b], Pathegama Gamage Ranjith [c], Bai-Cun Yang [d, **], Tian-Qiao Mao [e], Yu Li [d]

[a] Key Laboratory of Ministry of Education on Safe Mining of Deep Metal Mines, School of Resources and Civil Engineering, Northeastern University, Shenyang, 110819, Liaoning, China
[b] Key Laboratory of Liaoning Province on Deep Engineering and Intelligent Technology, Northeastern University, Shenyang, 110819, Liaoning, China
[c] Deep Earth Energy Laboratory, Building 60, Monash University, 3800, Melbourne, Victoria, Australia
[d] School of Resources and Civil Engineering, Northeastern University, Shenyang, 110819, Liaoning, China
[e] Key Laboratory of Shale Gas and Geoengineering, Institute of Geology and Geophysics, Chinese Academy of Sciences, Beijing, 100029, China

ARTICLE INFO

Article history:
Received 20 August 2024
Received in revised form
8 January 2025
Accepted 15 January 2025
Available online 17 January 2025

Edited by Yan-Hua Sun

Keywords:
Continental shale oil
Mechanical properties of different lamination types
True triaxial compression test
Structure control mechanism
Fracability evaluation

ABSTRACT

Clarify the mechanical properties of different laminations and the fracture mechanism of continental shale under in-situ stress can provide theoretical basis for more comprehensive evaluation of the fracability of continental shale oil reservoir. The Chang 7_2 continental shale was used to investigate the mechanical properties of laminations and the effect of natural structure on the crack propagation of the shale. The XRD and thin section tests show that the laminations contain two types: bright sandy lamination with void structure and dark muddy lamination with layer structure. The real-time CT uniaxial compression tests were conducted to investigate the differences of mechanical properties between the muddy lamination and sandy lamination. It found that the uniaxial compression strength and elastic modulus of the sandy lamination are higher, forming a simple crack with large opening, and the Poisson's ratio of the muddy lamination is large, forming obvious lateral deformation and more secondary cracks. On this basis, the cuboid-shaped continental shale specimens were tested under true triaxial compression conditions to study the effect of laminations and interface cracks on crack propagation combining AE and CT techniques. It found that nascent cracks connected laminations and interface cracks to form fracture network under appropriate loading condition, tensile cracks developed in sandy lamination and shear cracks occurred in muddy lamination because of deformation dissonance and brittleness index differences, and more secondary cracks formed in muddy lamination with smaller fracture toughness. Moreover, the combination relationships between nascent and natural cracks mainly conclude direct penetration and deflection, which is affected by the filling degree and morphology of interface cracks and the relationship of lamination types. These conclusions show that laminar continental shale is conducive to forming complex fracture network, which can provide a theoretical basis for the proposal of indicators and methods for fracability evaluation.

1. Introduction

Shale oil is abundant in geological resources in the world, which has become the principal part of international crude oil production growth. Strengthening shale oil exploration and development is an important way to ensure the security of national energy supply. Due to the geological characteristics of low permeability and significant brittleness of shale reservoirs, the fracturing technology has become an essential technology, and the fracability of the reservoir should be evaluated before using this technology (Sun et al., 2024; Zhao et al., 2025). Many scholars (Chandler et al., 2016; Yuan et al., 2017; Wang et al., 2019, 2020; Gupta et al., 2020; He et al., 2022; Yang et al., 2023) have paid attention to the mechanical properties and parameters of shale, such as elastic modulus, brittleness index, and fracture toughness through laboratory mechanical tests, in order to use more comprehensive indexes to evaluate the fracability of shale. Therefore, the study of

* Corresponding author.
** Corresponding author.
E-mail addresses: duanyongting@mail.neu.edu.cn (Y.-T. Duan), yangbaicun@mail.neu.edu.cn (B.-C. Yang).

https://doi.org/10.1016/j.petsci.2025.01.006

rock fracture mechanism of shale reservoir can directly clarify the deformation and fracture law of shale reservoir and provide mechanical parameters for rock fracability evaluation.

The shale oil development in the United States has made major breakthroughs, while the exploration of shale oil in China started is relative late and mainly oriented towards continental basins (Yang et al., 2019; Hu et al., 2020; Li and Chen, 2021; Bao et al., 2023; Chen et al., 2024a). Recent studies (Zhao et al., 2020; Sun et al., 2021; Zhang et al., 2022a; Zou et al., 2022; Guo et al., 2023; Bian et al., 2023; Jia, 2024) show that there are huge differences in geological conditions between China's continental shale oil and America's marine shale oil, which determines that the evaluation index and method of fracability of the marine shale cannot be used directly. Continental shale in China are highly heterogeneous, and the main shale types include laminar, layer and pure shale, among which the laminar continental shale has the best oil content (Jin et al., 2021; Shi et al., 2022; Xu and Gou, 2023). Currently, most fracability evaluation methods of continental shale reservoir refer to those of marine shale reservoir, and rarely consider the influence of the characteristics of continental shale oil reservoir, which results that the fracturing results of continental shale reservoirs are not ideal. Therefore, it is urgent to clarify the rock fracture mechanism affected by laminations, and provide a theoretical basis for the proposal of indicators and methods for fracability evaluation for laminar continental shale reservoir rocks.

Lamination refers to the smallest or thinnest structure units in shale oil enrichment and plays an important role in high shale oil production (Li et al., 2019a, 2022a; Xia et al., 2021; Shi et al., 2022). For the study of lamination characteristics of continental shale, some scholars have carried out studies to delineate the types of lamination, Xi et al. (2020) analysed the type of lamination based on the mineral composition of the lamination and other factors in the Chang 7 shale, and found that four major types of laminae, tuff-rich lamina, organic-rich lamina, silt-sized feldspar-quartz lamina and clay lamina, were mainly developed in the organic-rich shale. Shi et al. (2022) divided the lamination of the Paleogene organic-rich shale in the Dongying Sag into two categories, and revealed that laminar shale with high laminar continuity exhibit higher porosity, permeability, and oil saturation values than shale with poor laminar continuity. Some other scholars have conducted studies of thickness and fractals, Li et al. (2019b) conducted a multiscale study of grain layers and natural fractures in shale reservoirs in the Ordos Basin, and found that the average thickness of grain layers and the study scale obeyed the power function distribution law by constructing 3-D geological structure models. Liu et al. (2019) calculated the thickness of silty lamination of the Qingshankou Formation shale, and found that the number of laminations whose thickness is greater than or equal to the thickness of single lamination is linearly correlated with the thickness of single lamination. Huang et al. (2020) statistically analysed the minimum laminations of the shales of the Yanchang Formation at different scales, and found that the thickness of the multi-scale laminations exhibited fractal characteristic. Woo et al. (2021) concluded that shale from different environmental backgrounds and deposition processes exhibit different shape characteristics such as uniform, discontinuous, wavy and lenticular. These studies mainly focused on the lamination types and geometric distribution of continental shale.

Moreover, the mechanical properties of different types of laminations of continental shale are also been investigated. Meng et al. (2021) studied the elastic modulus, hardness, and fracture toughness of continental shale from four typical continental shale basins using the mineral analysis and nanoindentation tests. Wang et al. (2022a) applied the nanoindentation method to study the mechanical and creep properties of the Yanchang Formation continental shale, and found a strong anisotropy of mechanical properties, strong creep behaviour and weak fracture toughness. Li et al. (2022b) studied the elastic modulus differences of stiffer layer (pyritic lamination), intermediate layer (sandy lamination), and soft layer (organic-rich lamination) in continental Chang 7 shale using micro-indentation technique, and demonstrated that the elastic modulus of laminations correlated well with the mineral compositions and the nanoscale elastic modulus of individual minerals. Cheng et al. (2024) used the nanoindentation method to quantitatively analyse the micro mechanical properties of three laminations with different lithofacies of shale in the Bohai Bay Basin and investigated the mechanical differences between the different laminations. These studies have clarified the differences in deformation parameters of different types of laminations, but the differences in strength and failure mode are still needed to be carried out.

In addition to the lamination property, the fracture mechanism of continental shale with different types of laminar assemblages is also under way. Some scholars have carried out the uniaxial compression (Huang et al., 2020; Zhang et al., 2022b), conventional triaxial compression (Xia et al., 2019; Liu et al., 2020a; Li et al., 2022c), Brazil (Wang et al., 2020, 2022b), and twisted-torsion tests (Zhou et al., 2022) of laminar continental shale, which clarified the influence of laminar structures on the growth of nascent cracks. However, the mechanical differences between laminations are few considered, and the field stress conditions of reservoir rocks are closer to the true triaxial loading conditions ($\sigma_1 > \sigma_2 > \sigma_3$), it is more practical to study the fracture mechanism of rocks under true triaxial loading. Even though many scholars have conducted true triaxial compression tests of granite (Feng et al., 2019; Jiang et al., 2021; Ma et al., 2023), sandstone (Zhang et al., 2020a; Gao et al., 2022; Chen et al., 2023), and layered rock (Lu et al., 2020; Liu et al., 2020b, 2023a), and confirmed the influence of loading conditions on the growth of nascent cracks, but for the laminar continental shale with complex structure, the fracture mechanism under true triaxial loading conditions are still not clear.

To detect the structural characteristics and structural evolution of rock under loading conditions, the X-ray computed tomography (CT) technology, as a non-destructive testing technique, can be well used to solve the problem. In addition to observing the structural changes of rocks before and after the true triaxial loading, the synchronous testing process of loading and scanning can be realized by combining CT scanning device with a special loading device (Duan et al., 2022a), which is called the real-time CT loading tests. At present, some scholars have used the real-time micro-CT uniaxial compression equipment to carry out the real-time scanning tests on mud shale (Shi et al., 2021; Lin et al., 2022), sandstone (Fan et al., 2022), and granite (Gao et al., 2021; Fan et al., 2023) to study the fracture evolution process of these rocks. However, for the structures or cracking evolution characteristics of laminar continental shale, especially for the deformation and fracture process of different types of lamination specimens, there are still no relevant studies using the real-time CT technology.

In view of this, this investigation selects the Chang 7 laminar continental shale to classify the lamination types by combining with the structural observation, XRD and thin section analysis results. On this basis, the real-time micro-CT tests of different types of laminations are carried out to obtain the deformation and failure characteristics, and the differences in mechanical properties of laminations are analysed. In addition, the true triaxial loading tests and CT scanning tests of laminar continental shale are carried out to analyse the influence of lamination characteristics on the deformation and fracture of continental shale qualitatively and quantitatively, to clarify the structural controlling mechanism of the fracture of laminar continental shale, and put forward to combine the natural structure and the in-situ stress to comprehensively evaluate the fracability of laminar continental shale.

2. Geological background and sample information

2.1. Geological background

Ordos Basin is a large intracontinental basin in China, which is commonly subdivided into six first-order structural units (Li et al., 2018; Liu et al., 2021; Duan et al., 2022b, 2024). It developed during the Mesoproterozoic and sediments accumulated up till the Tertiary with an average thick 4–5 km, and it is a gentle, west-dipping monocline with dip angles less than 1° (Yang et al., 2016; Wang et al., 2017a; Pu et al., 2023). The Upper Triassic Yanchang Formation recorded a complete evolutionary cycle of a large lacustrine system and is 200–1400 m thick, which can be subdivided into ten oil layer groups that named Chang 1 to Chang 10 from top to bottom (Fig. 1(a)). The sedimentary period of Chang 7 Member is the largest stage in the deep lake area of the Yanchang Formation, and can be subdivided into three members: the Chang 7_1 Member, the Chang 7_2 Member, and the Chang 7_3 Member (Fu et al., 2020; Huang et al., 2020; Lyu et al., 2022; Mi et al., 2023). Controlled by semi-deep lacustrine to deep lacustrine deposition, the rocks in Chang 7 reservoir are characterized by strong heterogeneity, especially the Chang 7_2 Member shows apparent lamination. To study the lamination characteristics and the fracture mechanical of continental shale, the Chang 7_2 shale core samples with laminar development taken from the scientific well JK04 were obtained. This well is located in Jinsuoguan Town, Tongchuan City, southern Ordos Basin, at a depth of about 124 m. The corresponding core information is shown in Fig. 1(b).

2.2. Sample processing and lamination observation

The shale core disintegrates under the action of water when using the conventional cutting sample preparation method, and the structure of continental shale is complex, it is very difficult to prepare the samples. And four cuboid samples with dimensions of 35 mm × 35 mm × 70 mm were prepared in the laboratory using waterless diamond wire cutting technology (Ozcelik et al., 2002), each cuboid sample having horizontal laminations (Fig. 2(a)). Thereafter, the initial structures of each sample are observed using the optical photography and super depth-of-field 3-D microscopic system. Fig. 2(a) shows four sides of a continental shale sample, which is mainly constituted by bright laminations and dark laminations. In order to further distinguish the differences in mineral composition and structure between the two types of lamination, the XRD tests and thin section analysis tests are conducted at the corresponding lamination positions (I and II in Fig. 2(a)). Fig. 2(b) shows the pie chart of mineral composition percentages of the two types of lamination, and Fig. 2(c) shows the microscope photos of thin section analysis, respectively. It can be seen that the main mineral contents in the dark lamination at position I are 39.7% clay minerals and 44.3% brittle minerals (quartz, feldspar, and dolomite), and the mineral composition of the bright lamination at position II is dominated by brittle minerals (81.0%), which is almost twice as much as the dark lamination (Fig. 2(b)). Moreover, the dark lamination is stratified with black organic matter and maroon/yellow clay mineral with obvious bedding structure as well as filled with some scattered quartz and pyrite, while the brittle mineral particles are dispersed in the bright lamination with obvious void structure (Fig. 2(c)). In view of this, the structural characteristics of the two laminations are different obviously, according to the differences in laminar colour, morphology, composition and structures, the laminations of continental shale in the study area are divided into two types: dark muddy lamination with bedding structure and bright sandy lamination with void structure (Fig. 2(d)).

3. Real-time micro-CT uniaxial compression test of two laminations

Most studies (Huang et al., 2020; Liu et al., 2020a; Zhang et al., 2022b; Li et al., 2022c; Zhou et al., 2022) found that laminar structure has a certain influence on the propagation of nascent fractures, but there are few correlation analyses on the mechanical differences between different laminations and their influence mechanism on the growth of nascent fractures. In view of this, the mechanical differences between the muddy lamination and the sandy lamination are first investigated.

3.1. Lamination specimens and experimental process

The miniature waterless wire-cutting device and the precision cutting-grinding machine were used to obtain the specimens from core samples with two laminations. Based on the requirements of testing equipment and reference to the existed uniaxial compression test of marine shale (Duan et al., 2019, 2022a), the shape and size of the sample is a cylinder with a diameter of 4 mm and a height of 8 mm, and the cutting direction was perpendicular to the horizontal lamination planes (Fig. 3(a)). Then the prepared lamination specimens were tested under uniaxial compression conditions using the real-time micro-CT device (Fig. 3(b)), which can realize the test process of loading and scanning, more detail information about this CT equipment combined with a loading equipment can be found in Duan et al. (2020). Fig. 3(c) shows the loading curves and the CT scanning steps of the two lamination specimens, it can be found that the uniaxial compression loads of sandy lamination are obvious larger than that of muddy lamination. Moreover, the muddy lamination was scanned before loading, at 600, 900, 1200 N, and after fracture (scanning steps 1–5 labelled on the red curve), the sandy lamination was scanned at the same loading conditions except for a more step at 1500 N (scanning steps 1–6 labelled on the blue curve). At each scanning step, a three-dimensional (3-D) reconstructed stereogram and some horizontal CT images can be obtained (Fig. 3(d)), the CT scanning work flow has been listed in Duan et al. (2019). The pixel size of the CT image is 11.27 μm × 11.27 μm, and the effective region (the internal structure is clearly visible) is the middle position of the specimen, which is chosen as the ROI (region of interesting) and corresponds to the CT image number (i) from 300 to 700.

3.2. Deformation and strength differences of two laminations

In terms of deformation differences, the deformation in the axial direction was measured directly during the loading of real-time uniaxial compression tests of two lamination specimens, but lateral deformation cannot be obtained directly due to the limited specimen size, and was therefore calculated indirectly through the perimeter change of the specimens. Firstly, the structural characteristics of the specimens obtained by CT scanning in the ROI were selected, and the specimen perimeters of muddy lamination specimen and sandy lamination specimen were counted for every 25 layers (every 10 layers around layer 500) at each scanning step, as shown in Fig. 4(a) and (b), from which it can be seen that, before the peak force, the lateral deformation (perimeter changing) in the whole statistical region of the two specimens both increased with the increase of loading stresses, while the deformation values of the muddy lamination specimen are more obvious, which indicates that the muddy lamination specimen is more easily to deform,

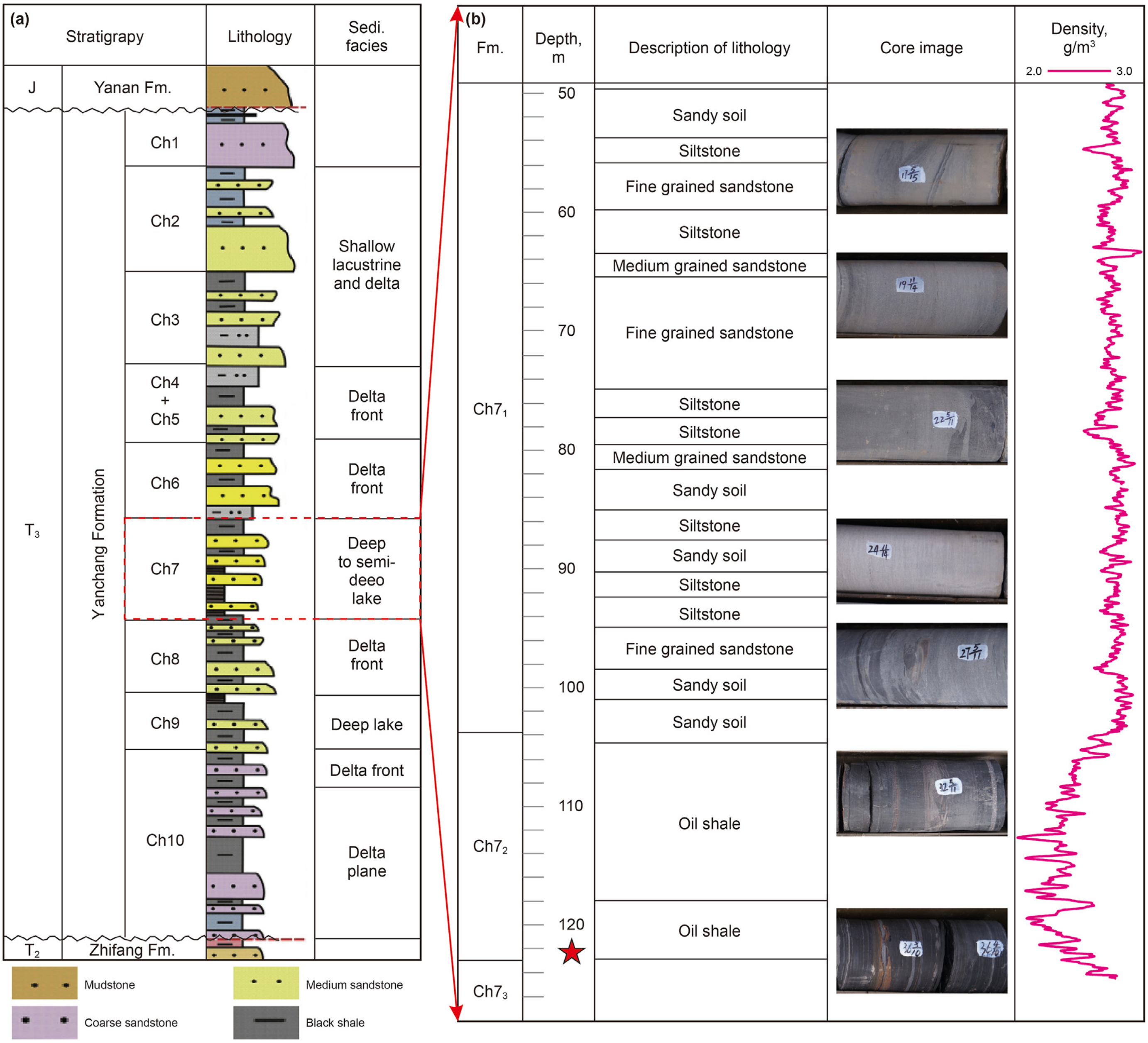

Fig. 1. Stratigraphic column of the Yanchang Formation (**a**) and the Chang 7 Member (**b**) (Modified after Wang et al. (2017a), Yang et al. (2017), and Li et al. (2018)). Ch = Chang; Fm. = Formation; Sed. = Sediment.

especially lateral deformation under the same force. Secondly, the average perimeter value of the ROI image was used to calculate the lateral strain, and then combined with the axial strain value to calculate the volumetric strain (Duan and Yang, 2022). Fig. 4(c) and (d) show the stress-strain curves (including axial strain, lateral strain and volumetric strain) of the muddy lamination specimen and sandy lamination specimen, respectively. It can be found that the axial strain and lateral strain of muddy lamination specimen are larger than that of sandy lamination specimen at each scanning step before the step 4, and the volumetric strain curve deviates more obviously from the straight line. When loading to the peak values, the lateral strain of muddy lamination specimen is still lager even though the axial strain values are almost the same.

For the deformation differences, the mechanical parameters of elastic modulus (E) and Poisson's ratio (μ) are also calculated, and the values are 10.94 GPa and 0.25 for the muddy lamination specimen as well as 13.24 GPa and 0.15 for the sandy lamination specimen. However, Li et al. (2022b) obtained the elastic modulus of organic-rich lamination and sandy lamination of similar samples through micro-indentation test, which is about 14.15 and 132.20 GPa, respectively. It found that the values obtained by real-time CT uniaxial compression test are smaller than that of micro-indentation test, especially for the elastic modulus of sandy lamination. On the one hand, the lamination specimen in the CT test contains the inner structure: the layered combination of muddy lamination (Fig. 5(d)) and the void structure of sandy lamination (Fig. 5(e)), which impacts the deformation characteristics of lamination specimens in the process of loading and reduces the elastic modulus value to a certain extent of the two types of laminations. On the other hand, there are a small number of low-density

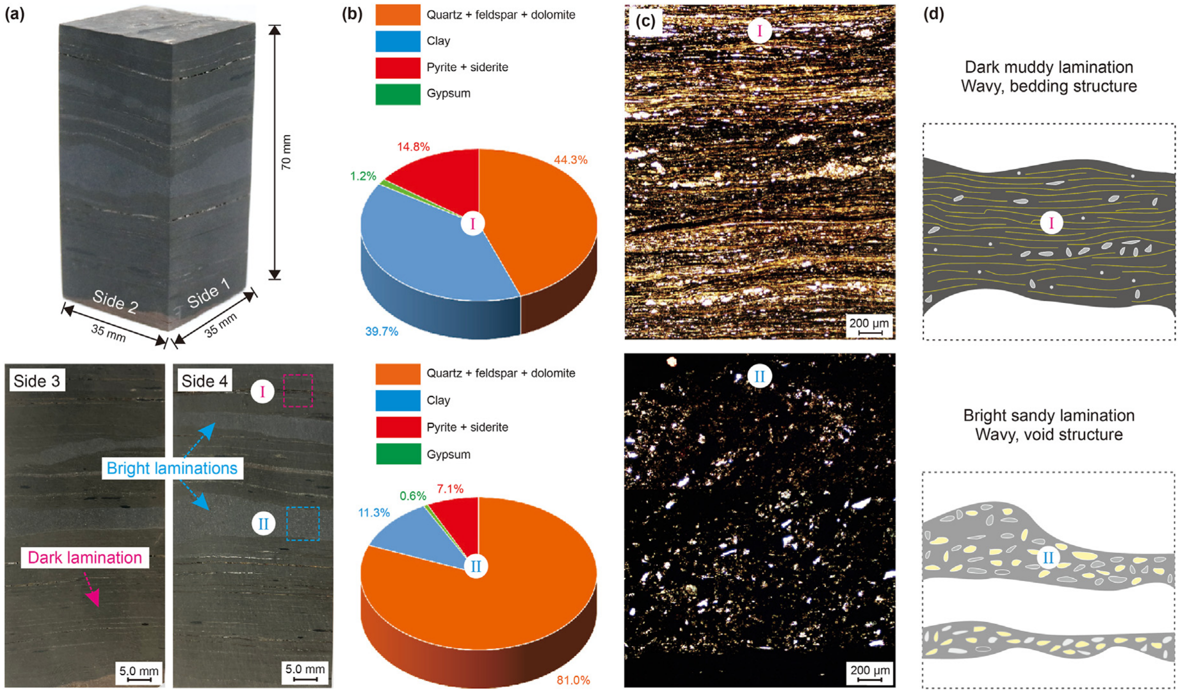

Fig. 2. Photos of one cuboid sample (**a**), pie chart of mineral contents (**b**), photos of thin section under single polarized light (**c**) and schematic diagrams (**d**) of two laminations at positions I and II.

interlayers in the sandy lamination specimen tested by real-time CT device (Fig. 5(e)), which also makes the elastic modulus of sandy lamination lower than the result of micro-indentation. In view of this, it is mainly due to the internal structural characteristics of the lamination specimen, the elastic modulus is lower than that of micro-indentation test. Although the elastic modulus of sandy lamination obtained by real-time CT test is slightly lower, it does not affect the accuracy of the analysis conclusions, especially when analyzing the influence of deformation, brittleness index and fracture toughness differences of two types of laminations on the propagation law of new fractures by comparing the elastic modulus of muddy lamination. Moreover, this value is thought to be more reasonable because the rock structural influences should be taken into account when measuring rock mechanical parameters.

For the strength differences, the uniaxial compression strength (UCS) is 98.67 MPa of the muddy lamination specimen and 115.51 MPa of the sandy lamination specimen, and the average value is 107.09 MPa. However, the UCS value of continental shale core (ϕ100 mm $\times$ 160 mm cylindrical specimen) of Chang 7_2 Member obtained by Zhao (2018) is 42.15 MPa. It found that the UCS value of continental shale core with two laminations combinations is smaller than the average UCS value of the two lamination specimens. And even under the triaxial loading tests in this study, the true triaxial compressive strength of laminar continental shale specimen is about 60 MPa, which is still lower than the average value of two laminations. This mainly due to the development of a large number of interface cracks in laminar continental shale, which controls the crack propagation pattern and greatly reduces the uniaxial and true triaxial compressive strength of continental shale specimens. It can be seen that in addition to the internal structural characteristics of laminations, the interface cracks jointed different types of laminations also have a great influence on the mechanical property parameters of laminar continental shale.

3.3. Failure mode differences of two laminations

Except for the mechanical parameters of two laminations, the failure characteristics of two lamination specimens can also be analysed. Fig. 5(a) and (b) show the 3-D reconstructed volumes by CT images of the two damaged specimens. It found that the cracks of the muddy lamination specimen have bifurcation phenomena, the fracture morphology is more complex and the number of cracks is slightly more than that of the sandy lamination specimen. To further analyse the differences in fracture morphology and the effect factors, the internal slices in three orthogonal directions of 3-D reconstructed specimens were observed (Fig. 5(c)), and the changing of internal structure characteristics of the two types of lamination specimens before loading and after failure were compared (Fig. 5(d) and (e)). The results show that the layered structure in the muddy lamination specimen and the brittle mineral particles in the sandy lamination specimen are visible in the CT slices before test. The layered structure that formed by clay minerals has a "guiding" effect on the propagation of new fractures, that is, the new fracture tends to extend along the interface of the layered structure, and there are oblique secondary cracks and the widths are small. The effect of void structure that formed by brittle minerals on the propagation of nascent fractures is similar to that of homogeneous rocks, that is, the new fracture forms a relatively straight inclined fracture with a larger width at the specimen end. It should be noted that there is a low-density mineral interlayer at the lower end of the sandy lamination specimen, which has a certain influence on the expansion of new fracture in the sandy lamination, making the fractures extend along the interlayer to the specimen boundary, this specific influence would be discussed in the discussion section. For the fracture differences of two lamination specimens, to sum up, the cracks in the muddy lamination have larger roughness, smaller average width and more complex overall morphology, and the roughness of cracks in the sandy lamination is smaller, the average width is larger, and the overall shape is more single.

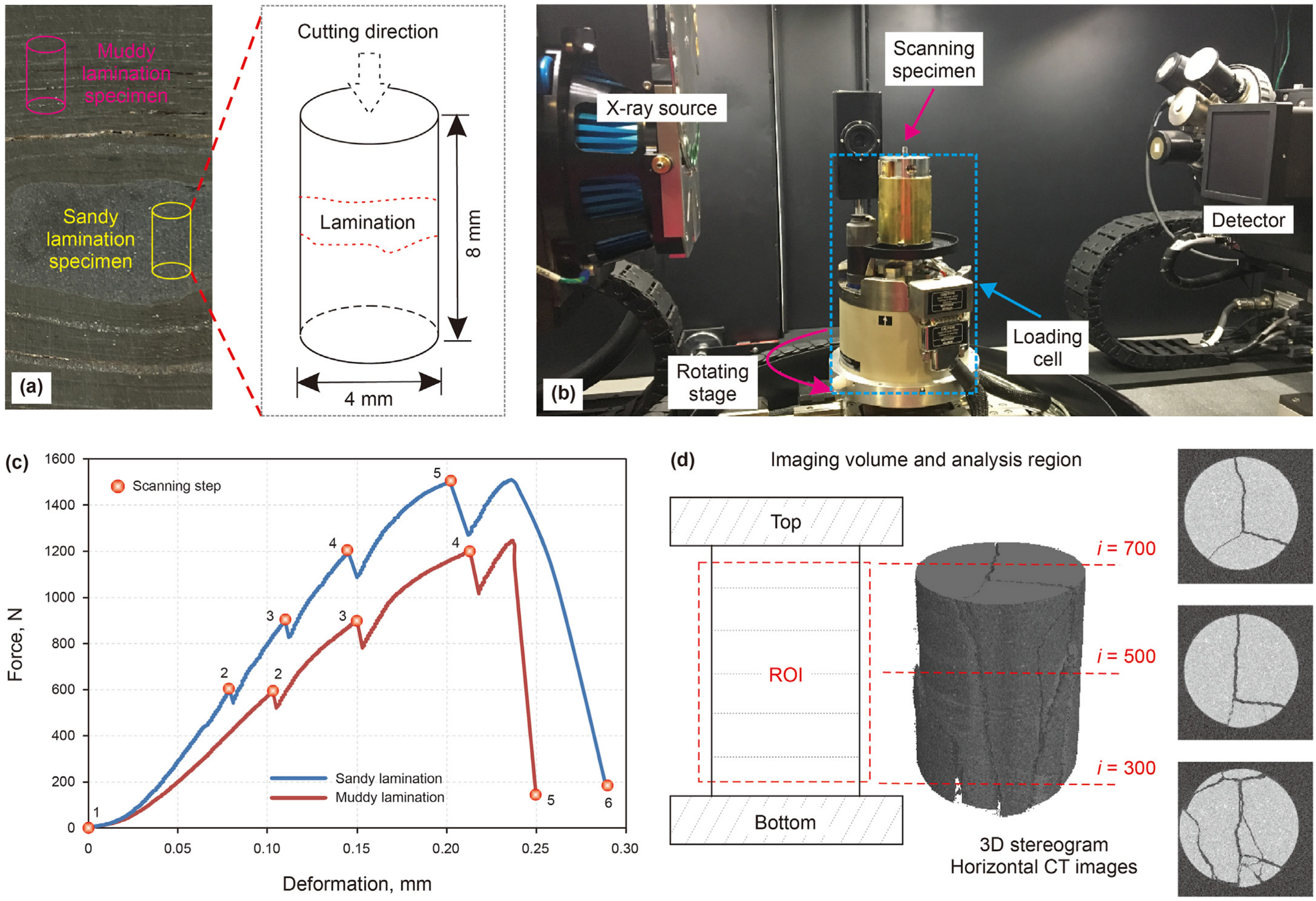

Fig. 3. Locations and schematic diagram of two lamination specimens (**a**), the real-time micro-CT device (**b**), the loading curves and scanning steps of two specimens (**c**), and the descriptions of CT results (**d**).

4. True triaxial compression tests of laminar continental shale

On the basis of clarifying the fracture characteristics of different types of laminations, it is more practical to study the influence mechanism of laminations on the growth of nascent fractures of continental shale with lamination combination, especially under real in-situ stress. Therefore, true triaxial compression tests were carried out on four cuboid shale specimens to analyse the damage evolution and fracture characteristics, and also the effect of natural structures on the crack propagation and failure mode were analysed.

4.1. Loading scheme and experimental process

Tests were carried out using a Mogi type true triaxial test system with a loading capacity of 100 MPa for the minimum principal stress (σ_3) and 1200 MPa for both the intermediate and maximum principal stresses (σ_2 and σ_1) for standard sized cubic specimens. Considering the core depth, the geological conditions of the sampling site and the carrying capacity of the loading device, the minimum principal stress σ_3 is selected as 5 MPa (Duan et al., 2024). Moreover, according to the research results of the field work, the horizontal geo-stress difference of the Chang 7 reservoir rocks in the Ordos Basin, which mainly develops laminar continental shale, is 6–12 MPa (Yuan et al., 2015), 5–7 MPa (Yang et al., 2015) and 4–5 MPa (Jiao, 2021). Consequently, the intermediate principal stress σ_2 in the conventional triaxial test is designed to be 5 MPa (S1) and in the true triaxial test are 10 MPa (S2), 15 MPa (S3), and 20 MPa (S4), and the maximum principal stress σ_1 is the value when the specimen fractured. To perform the test, the tested specimen was secured by two pairs of clamps and placed horizontally (the long axis is in the horizontal direction and corresponds to the σ_1 loading) in the pressure chamber, where various force and deformation sensors were connected, and then the chamber was pushed into the loading frame for loading test. The prepared continental shale specimens in this study were tested under conventional triaxial ($\sigma_1 > \sigma_2 = \sigma_3$) and true triaxial ($\sigma_1 > \sigma_2 > \sigma_3$) compression conditions, the axial force and displacement parameters in three orthogonal loading directions were recorded. The loading mode of all specimens is strictly in accordance with the testing standards recommended by Feng et al. (2019).

4.2. Analysis of acoustic emission (AE) monitoring results

The crack initiation and crack propagation under in-situ geological stress are of particular importance to reveal the failure mechanism of shale and to use these two thresholds (crack initiation stress (σ_{ci}) and peak stress (σ_c)) in engineering practice (Li et al., 2020). During the true triaxial compression loading, in addition to monitoring the force and displacement values, the AE sensor is also used to monitor the evolution of acoustic signals to characterize the rock damage evolution. The evolution

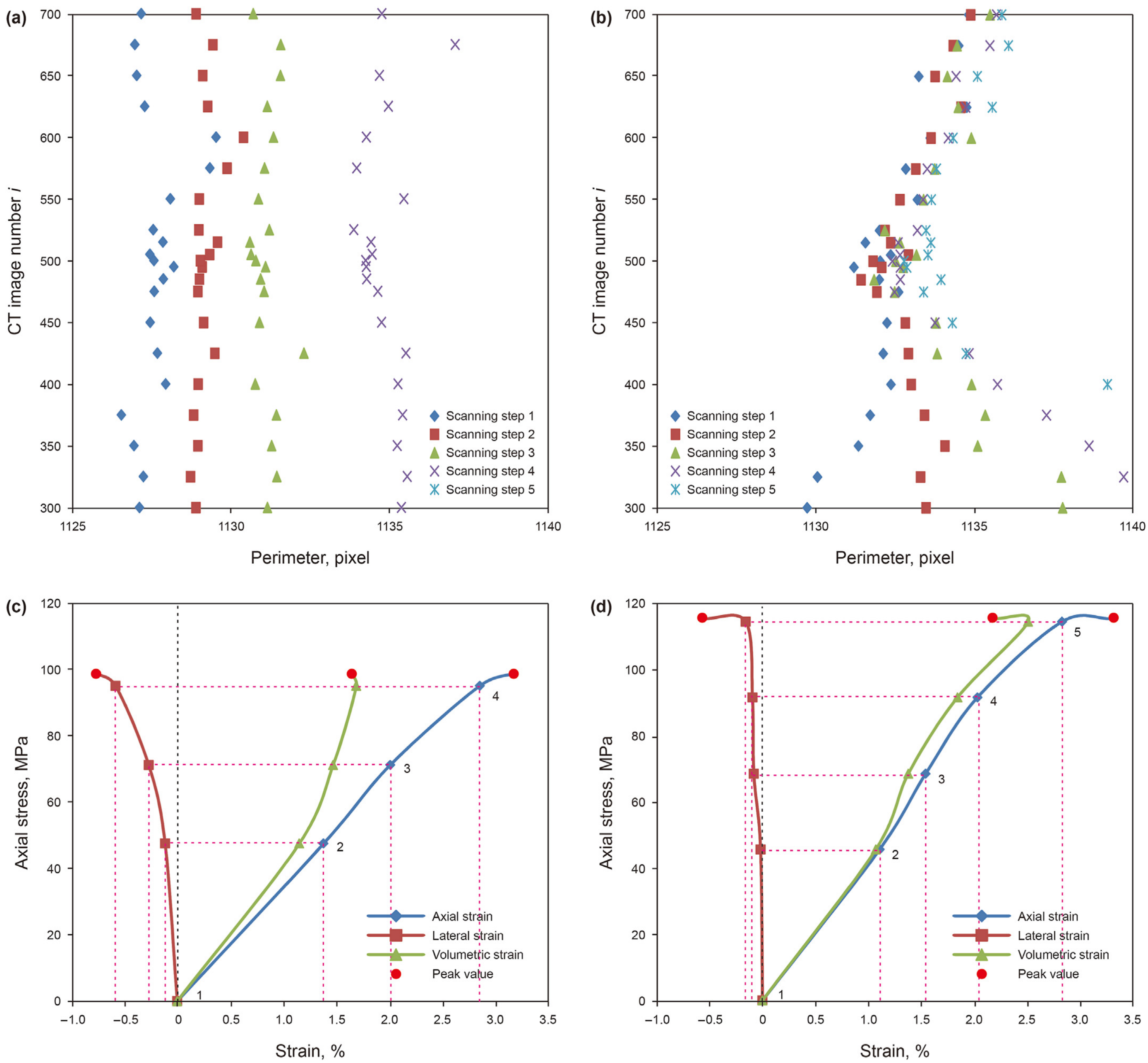

Fig. 4. Evolution of specimen perimeter of muddy lamination (**a**) and sandy lamination (**b**) specimens as well as stress–strain curves of muddy lamination (**c**) and sandy lamination (**d**) specimens.

characteristics of differential stress ($\sigma_1-\sigma_3$) curve, AE ring count and cumulative AE ring count curve of S3 and S4 are shown in Fig. 6(a) and (b). It found that a lot of AE ring counts occurred before the peak strength and included two large AE ring counts, and two corresponding sudden increases appeared in the cumulative AE ring count curve of each specimen. To describe the damage evolution characteristics quantitatively, according to Kachanov (1958), Rabotnov (1963) and Li et al. (2019c), a damage variable D by taking into the cumulative AE ring counts is defined as:

$$D=\frac{C_\mathrm{d}}{C_0} \tag{1}$$

where D is the damage variable; C_d is the cumulative AE ring counts; and C_0 is the cumulative AE ring counts of the completely damaged section.

By combining the stress evolution curve, damage variable curve, AE count characteristics, and cumulative AE ring count curve, the damage evolution of continental shale under true triaxial loading condition can be considered experienced the stable crack extension stage and the unstable crack propagation stage. Then according to the suggested method of Zhang et al. (2020b) and Wu et al. (2023), the two stress thresholds can be determined. As shown in Fig. 6, the first sudden increase in cumulative AE ring count curve at point A corresponds to the crack initiation stress (σ_ci) and the second one at point B is related to the damage stress (σ_cd). Then the ratios of each stress threshold to the peak stress (σ_c) can be calculated, correspondingly, the ratios of $\sigma_\mathrm{ci}/\sigma_\mathrm{c}$ and $\sigma_\mathrm{cd}/\sigma_\mathrm{c}$ are calculated to be 52.6% and 78.1% for S3 as well as 56.4% and 61.7% for S4. It found that with

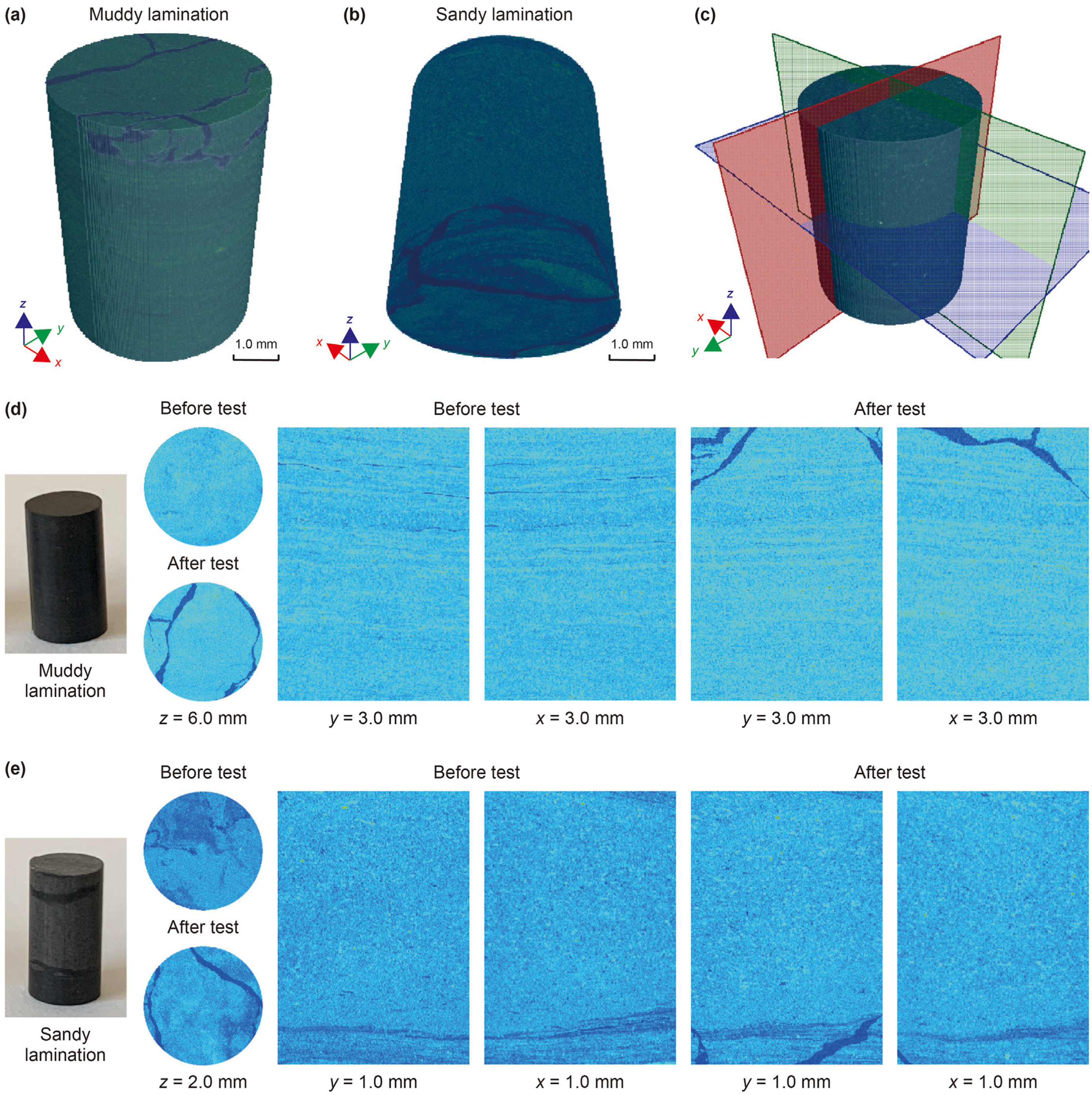

Fig. 5. Failure mode of muddy lamination (**a**) and sandy lamination (**b**), the schematic diagram of internal slices (**c**), and CT results of muddy lamination (**d**) and sandy lamination (**e**) before and after test.

the increase in intermediate principal stress, the stress ratios show a slight increase but the degree is limited, which indicates that the intermediate principal stress has little influence on the damage evolution of continental shale. In addition, the research results of Xue (2015) showed that the value of σ_{cd}/σ_c of sedimentary rocks under uniaxial compression condition is about 80%, which is higher than the two values (78.1% and 61.7%) of continental shale in this study. Noted that the loading condition in this study is true triaxial compression, the confining pressure should inhibit the crack development and increase the stress ratios of σ_{ci}/σ_c and σ_{cd}/σ_c (Kong et al., 2018). However, the σ_{cd}/σ_c values of continental shale under true triaxial compression condition are smaller than that under uniaxial compression condition. This is mainly due to the influence of the initial structure of continental shale, and the specific controlling mechanism is analysed in detail in Section 5.

4.3. Deformation and strength characteristics and failure mode analysis

Fig. 7 shows the testing results of the relationships between differential stress ($\sigma_1-\sigma_3$) and principal strain (ε_1, ε_2, and ε_3), as well as the corresponding photos of four fractured specimens of S1, S2,

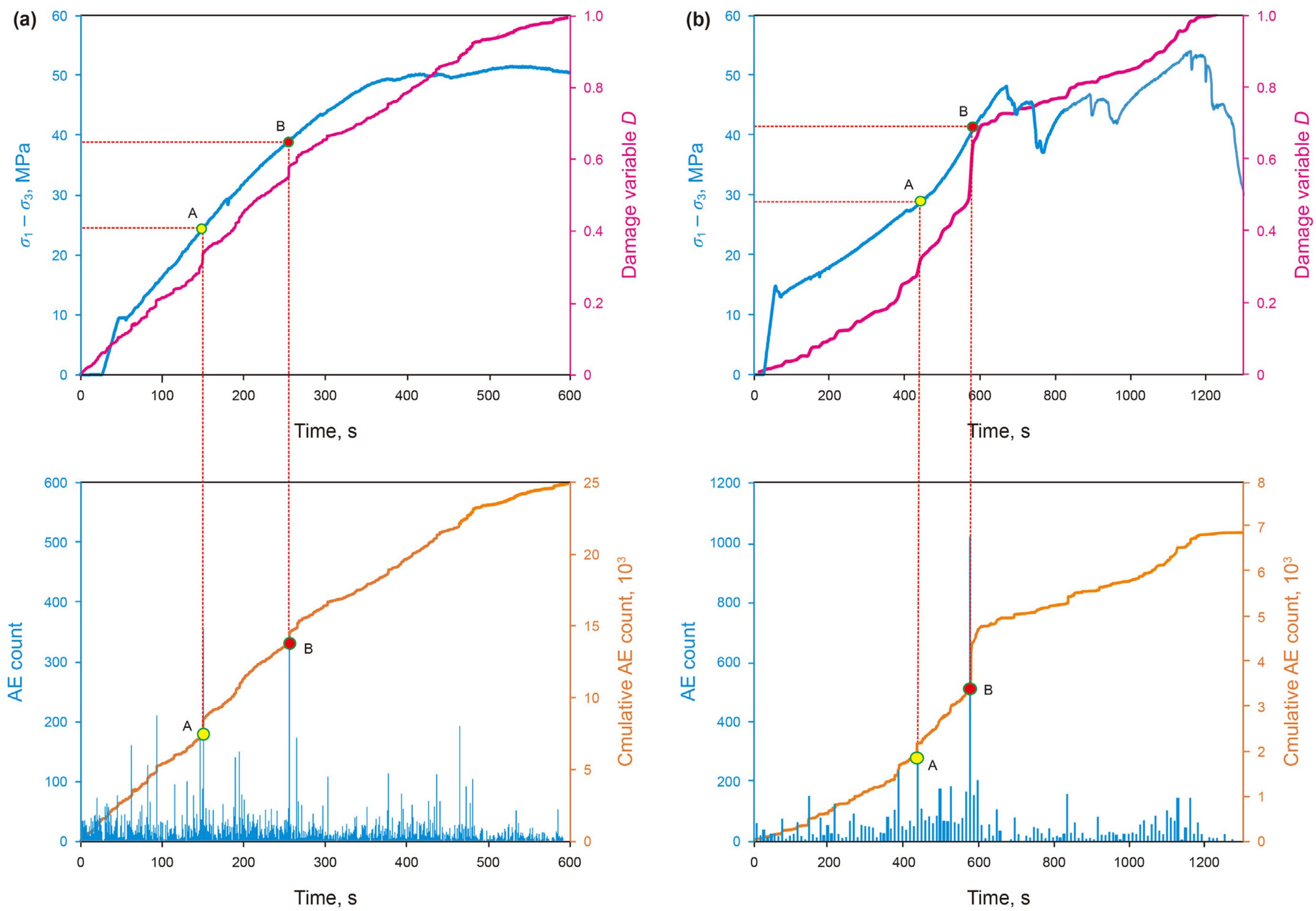

Fig. 6. Evolution characteristics of differential stress curve, damage variable curve, AE ring count and cumulative AE ring count curve of S3 (**a**) and S4 (**b**).

S3 and S4. For the deformation characteristics, the morphology of S2, S3, and S4 curves is of the type of elastic-plastic-brittle multi drop (EPB-M), all of which show multiple drops and rises after the stress peaks. On the one hand, as the intermediate principal stresses increase, the ε_2 curves change from expansion to compression and the development trend becomes steeper and steeper, so the deformation modulus in the ε_2 direction becomes larger and larger. On the other hand, the ε_3 curve is always expanding and the development trend is getting flatter and flatter, so the deformation modulus in the ε_3 direction is getting smaller and smaller. Combining the curve changes under different loading conditions, it can be seen that under the true triaxial stress, the intermediate principal stress plays a limiting role on the deformation of the rock, and the deformation of the rock in the direction of the intermediate principal stress and the minimum principal stress shows obvious stress-induced deformation anisotropy.

For the strength characteristics, the peak strength of shale specimens has a non-linear change characteristic, which may be related to the complex structure of continental shale. Under the condition of constant minimum principal stress, the peak strength of the sample decreases first and then increases asymmetrically with the increase in the intermediate principal stress, but the difference between the four test results is in the range of about 5 MPa. The enhancement coefficient λ (Eq. (2)) can be calculated to quantify the percentage enhancement of the peak stress by the stress difference (Feng et al., 2020; Feng and Yang, 2023):

$$\begin{cases} b=\dfrac{\sigma_2-\sigma_3}{\sigma_1-\sigma_3} \\ \mu=2b-1 \\ \lambda=\dfrac{\sigma_\mu-\sigma_{\mu=-1}}{\sigma_{\mu=-1}} \end{cases} \tag{2}$$

where b denotes the intermediate principal stress coefficient of rock; μ denotes the stress Lode parameter; σ_μ denotes the peak strength of rock at different intermediate principal stress states, when $\mu=-1$, it means that the rock is in the generalized triaxial compression state (i.e. conventional triaxial compressive state). The calculated results of the enhancement coefficients λ are 9.57%, 0.49%, and 4.68% for S2, S3, and S4 in the true triaxial condition, while the λ for hard rocks such as sandstone is generally 20% (Feng and Yang, 2023), which in summary can indicate that the intermediate principal stress has less influence on the peak strength for continental shale. However, for the crack initiation strength, it can be obtained that the σ_{ci} of S3 and S4 are 29.76 and 33.23 MPa, the crack initiation strength increases with the increase in intermediate principal stresses, which shows that the intermediate principal stresses can affect the crack initiation strength. Due to the increase in intermediate principal stresses, the pore space and interstices of the particles inside the rock are continuously reduced, which increases the occlusion force between the internal particles of rock,

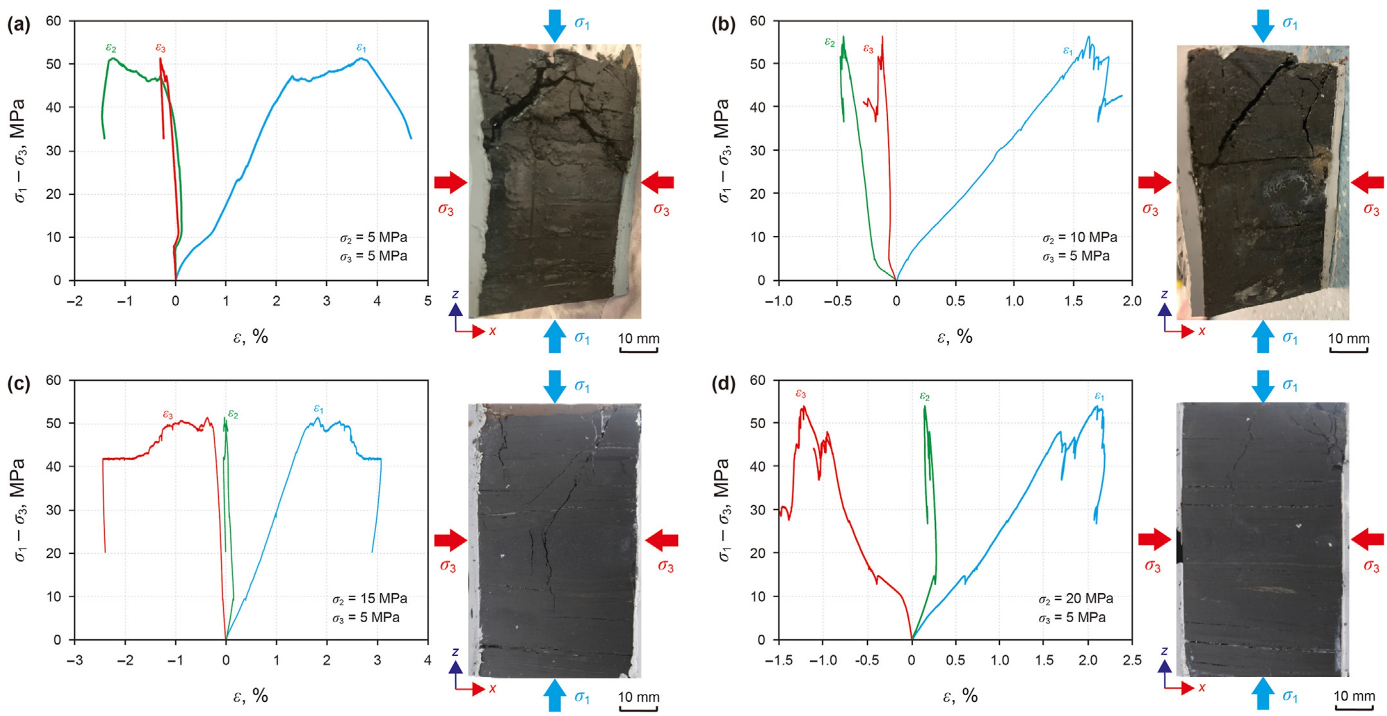

Fig. 7. Differential stress vs. principal strain curves and fractured specimen photos of S1 (**a**), S2 (**b**), S3 (**c**), and S4 (**d**).

and the internal densification becomes more compact. This process requires a greater stress to produce the nascent microcracks, and thus the crack initiation strength has been improved.

For the failure characteristics, to characterize the internal mesoscopic structures of four continental shale specimens before and after the true triaxial compression tests, the non-destructive 450 kV industrial X-ray CT system (Sun et al., 2020) was employed. Therefore, a reconstructed 3-D stereogram and some slices can be obtained for each CT scanning (each specimen scanned twice times: before and after test), and the pixel size of these CT results is 0.129 mm × 0.129 mm. Fig. 8 shows some rendered CT results (including 3-D volumes and CT slices in three orthogonal directions) of S3 before test and those of S1, S2, S3, S4 after test. Before test, it can be found that the density differences of sandy lamination (high density with orange-red colour) and muddy lamination (middle density with green colour) according to the imaging principle of CT images, and a large number of natural cracks (low density with blue colour) can also be observed (Fig. 8(a)). These initial structures have a certain influence on the failure results of the specimen. After test, it can be seen that a complex new fracture developed at the upper end of S1 that under conventional triaxial loading (Fig. 8(b)) because the fracture features can be observed in both the x–z ($y = 15$ mm and $y = 25$ mm) and y–z ($x = 15$ mm and $x = 25$ mm) planes and are obvious, while the trend of new cracks of S2, S3, and S4 that under true triaxial compression condition (Fig. 8(c)–(e)) is mainly along the σ_2 loading direction (y-axis direction) and the fracture features observed on the y–z planes ($x = 15$ mm and $x = 25$ mm) gradually decrease from S2 to S4. This is due to the fact that as the intermediate principal stress coefficient b increases, the fracture anisotropy gradually increases and the angle between fracture surface and σ_2 direction becomes smaller and smaller, so that the decreasing fracture features can be observed gradually in y–z planes. Moreover, the inclined main fractures and a large number of secondary cracks formed in the muddy lamination, the vertical main fractures developed in the sandy lamination and the number of them is small. The macroscopic main cracks are mainly in the form of steps with alternating vertical and inclined cracks, showing a mixed tensile-shear damage mode of "vertical-inclined-vertical penetration". And the degree of connection of the new cracks to the natural cracks was generally more pronounced, with a variety of connections such as penetrations, "brick" laying and flexures, with the best degree of penetration in the S3 surface cracks. More information about the effect of lamination types and natural fractures on fracture propagation, see Sections 5.1 and 5.2.

These laboratory results of true triaxial loading show that a complex fracture (lager vertical penetration degree, combination of inclined and vertical cracks, main and secondary cracks) can be formed in continental shale under an appropriate stress difference condition (S2 and S3, horizontal stress difference (σ_2–σ_3) is 5 and 10 MPa), which indicates that the combination of different laminations (muddy lamination and sandy lamination) and natural fractures is conducive to the formation of fracture network system. Therefore, the in-situ combination characteristics of geo-stress and structure of Chang 7 reservoir have a positive contribution to promote the establishment of reservoir rock fracability evaluation model.

5. Discussion

In field work, a good hydraulic fracturing result is the formation of a complex stimulated reservoir volume (SRV) in the shale reservoirs, but its formation is premised on the formation of a complex fracture in the shale mechanics test samples tested in laboratory (50% contribution). Studies (Huang et al., 2019; Xu and Gou, 2023) demonstrated that the process of producing a fracture system is not only related to the shale's mechanical parameters, such as the compressive strength, elastic modulus, and tensile strength, but also the shale's texture. The two factors control the generation of micro-cracks and crack propagation, and then determine the complex degree of shale fracture. Laminar continental shale in this study is formed by alternating sandy lamination and muddy

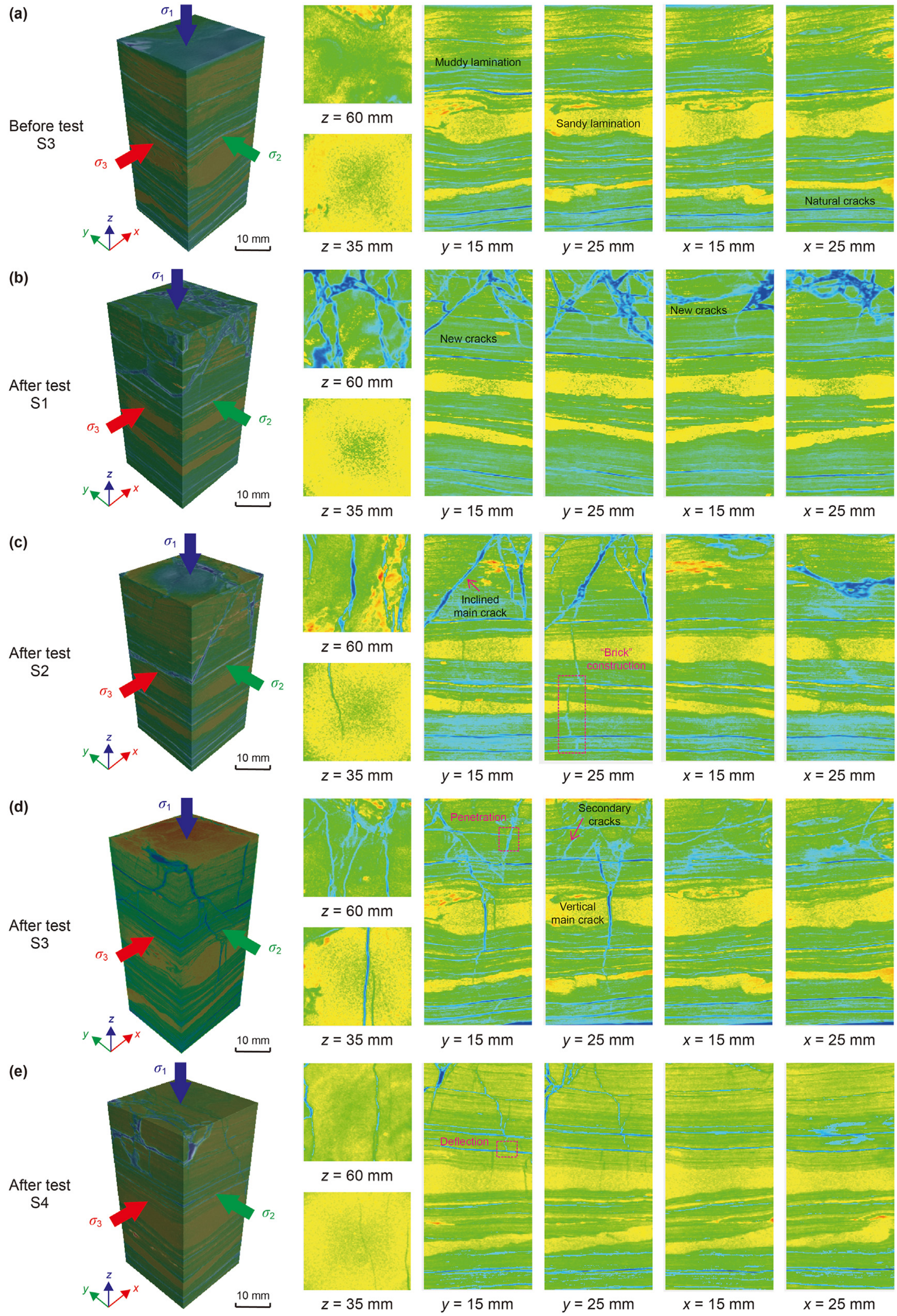

Fig. 8. CT scanning results (3-D volumes and CT slices in three orthogonal directions) of S3 before test (**a**), and S1 (**b**), S2 (**c**), S3 (**d**), and S4 (**e**) after test.

lamination as well as some interface cracks, which enhances the heterogeneity of the rock's physical and mechanical properties, that controls the failure mechanism, and also affects the comprehensive evaluation of the fracturing capacity of laminar continental shale.

5.1. Effect of lamination types on the crack propagation

It shows that the mineral composition and structure of muddy lamination and sandy lamination are different obviously in Section 2.2, which results in the differences of mechanical parameters of the two types of laminations in Section 3, then the influence of lamination types on new fracture type can be analysed. The E and μ are 10.94 GPa and 0.25 of the muddy lamination as well as 13.24 GPa and 0.15 of the sandy lamination, which indicates that sandy lamination exhibits the higher compressive strength and elastic modulus and the lower Poisson's ratio. Therefore, during true triaxial loading, the muddy lamination is as the relatively softer interlayer and tends to making more transverse deformation, which is equivalent to the muddy lamination applying a transverse tensile force at the upper and lower interfaces of the sandy lamination (red arrows in Fig. 9(a) and (b)). As a result, the "I" type fracture with greater opening is formed within the sandy lamination (Fig. 9(c)). As the rupture plane is perpendicular to the laminar surface, and the upper and lower boundaries of sandy lamination have no dislocation, indicating that the fracture is a tensile crack. Moreover, the undulation pattern of sandy lamination contributes to the stress heterogeneity positively at the boundary of laminations, and then induces the tensile fracture steering. On the contrary, the sandy lamination is as the relative stiffer interlayer, the deformation of the muddy lamination is limited by the sandy lamination, which is equivalent to the sandy lamination applying a transverse compression force at the upper and lower interfaces of the muddy lamination (blue arrows in Fig. 9(a) and (b)), resulting in the appearance of "V" type inclined crack in the muddy lamination. As the rupture plane is oblique at the laminar surface, and the nearly horizontal natural crack in the muddy lamination experiences dislocation after the test (Fig. 9(c) and (d)), thus the shear fractures are formed within the muddy lamination. In summary, it can be seen that the deformation dissonance between the two types of laminations has a controlling effect on the formation type of new fractures.

On this basis, in order to distinguish the brittle-plastic fracture characteristics of two laminations quantitatively, the brittleness index B_{rit} of two lamination specimens is then calculated. Actually, there are various methods to calculate the brittleness index of reservoir shale rock (Wang et al., 2017b; Gu et al., 2021; Yang et al., 2022, 2023; Xia et al., 2022), which is partly based on the content of brittleness mineral of rocks, partly based on the differences in rock mechanical properties. Because the mechanical parameters are the comprehensive performance of mineral composition and structure combination of rock, the method proposed by Rickman et al. (2008) that the brittleness index can be calculated with rock mechanical parameters (Eq. (3)) is used.

$$\begin{cases} Y = \dfrac{Y_{\mathrm{c}} - 1}{8 - 1} \times 100 \\ P = \dfrac{P_{\mathrm{c}} - 0.4}{0.15 - 0.4} \times 100 \\ B_{\mathrm{rit}} = \dfrac{Y + P}{2} \end{cases} \tag{3}$$

where Y_{c} is the static Young's modulus, 10^4 MPa; P_{c} is Poission's ratio; Y is the brittleness calculated from the Young's modulus; P is the brittleness calculated from the Poisson's ratio; and B_{rit} is the brittleness index.

The results show that the brittleness index of sandy lamination is 52.31, and that of muddy lamination is 30.67, which is in line with the research conclusion of Yang et al. (2022) that the brittleness index for Chang 7 shale is from 7.46 to 65.69. In view of this, combined with the conclusion of Qin et al. (2016) that the rock stratum with brittleness index greater than 40 can be classified as brittle fracturing segment, the sandy lamination is then regarded as brittle layer and the muddy lamination is regarded as plastic layer. Therefore, combined with the minimum energy principle, the new fractures tend to take the shortest path in the brittle sandy lamination (forming the vertical tensile fracture), on the contrary, the new fractures in the plastic muddy lamination tend to take the longest path (forming the inclined shear fractures) (Fig. 9(c)). In view of this, it can be seen that the brittleness difference between two types of laminations also affects the type of new fractures.

Expect for the fracture type, the number of new fractures in two

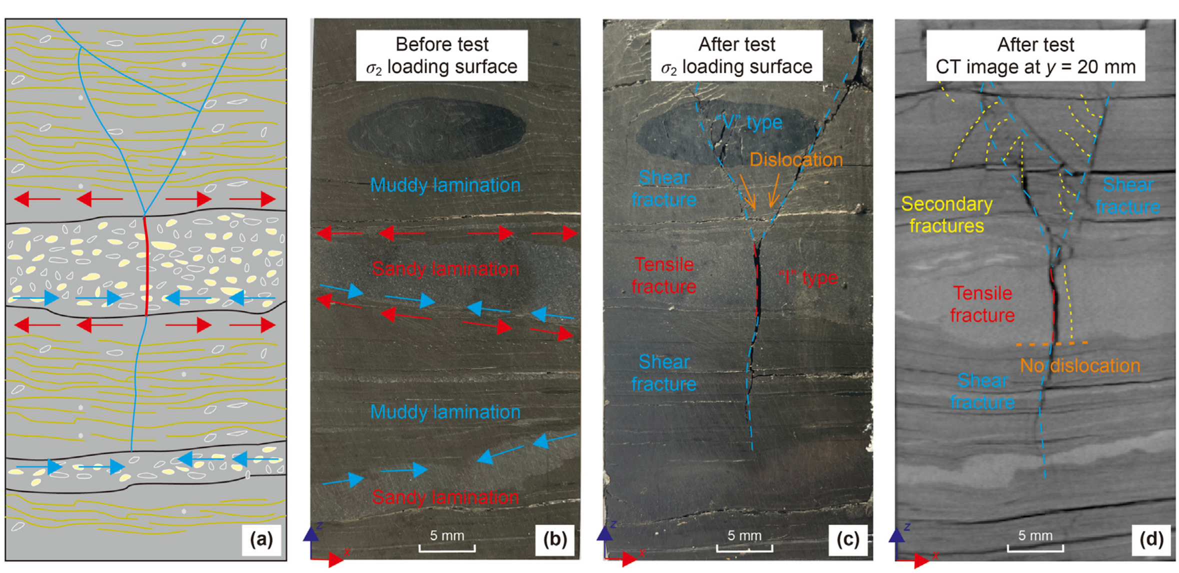

Fig. 9. Schematic diagram of deformation dissonance between two laminations (**a**), photos of specimen surface before (**b**) and after (**c**) test, and a CT image (**d**) of damaged S3.

laminations is also different. It can be found that more secondary fractures formed in the plastic muddy lamination, and the morphology of secondary fractures is more complex, intersecting with the main fracture at different angles (Fig. 9(d)). In other words, the lamination types also have influences on the complexity of nascent fractures. In quantitative analysis aspect, the difficulty of crack propagation is related to the fracture toughness of the rock in fracture mechanics theory, and in general, the smaller the fracture toughness, the easier the propagation of cracks (Huang et al., 2019; Gupta et al., 2020; Meng et al., 2021; He et al., 2022), thus the plastic muddy lamination with smaller fracture toughness is more prone to crack. On the one hand, Liu et al. (2016) and Zhang et al. (2024) pointed out that the fracture toughness is proportional to the elastic modulus of rocks. And the test results in this study show that the elastic modulus of sandy lamination is greater than that of muddy lamination. Therefore, it can be concluded that the fracture toughness of muddy lamination is smaller, and the secondary cracks are more likely to form inside it. On the other hand, Huang et al. (2019) given the fitting formula (Eq. (4)) for calculating the fracture toughness based on the mineral composition contents of rocks.

$$\begin{cases} K_{\mathrm{Ic}} = -0.45Q_z - 0.47C_l + 0.25C_s + 0.5272 \\ K_{\mathrm{IIc}} = -1.04Q_z - 1.16C_l + 0.53C_s + 1.4737 \end{cases} \tag{4}$$

where K_{Ic} is the mode-I fracture toughness; K_{IIc} is the mode-II fracture toughness; Q_z is the quartz content; C_l is the clay content; and C_s is the siderite content.

Combined with the mineral results of two types of laminations in this study, the K_{Ic} and K_{IIc} are 0.39 and 1.14 MPa m$^{0.5}$ of sandy lamination as well as 0.22 and 0.73 MPa m$^{0.5}$ of muddy lamination. Therefore, it found that K_{IIc} is roughly three times that of K_{Ic} (Gupta et al., 2020), more importantly, the fracture toughness of muddy lamination is smaller, namely its ability to resist damage is smaller, and then more secondary cracks formed inside it. In summary, it can be seen that the fracture toughness index of two types of laminations controls the number of new fractures.

Considering the deformation parameters, brittleness index and fracture toughness of two types of laminations, the differences of types and the number of new fractures are analysed, and then the fracability of continental shale that discussed in Section 5.3 can be evaluated. In conclusion, the tensile fractures are easier to form within the brittle sandy lamination and the number of fractures is single, and the shear fractures are easier to form within the plastic muddy lamination and more secondary fractures are likely to develop. These results indicate that the sandy lamination and muddy lamination have different controlling mechanism on the propagation of new fractures, thus the combination of different laminations is conducive to the formation of complex fracture networks in continental shale, which means the laminar continental shale has effective fracability and is a favorable fracturing lithofacies.

5.2. Interface cracks effect on the crack propagation

In the study of fracture propagation of continental shale, in addition to paying attention to the influence of lamination type on reservoir heterogeneity, the interface cracks that can provide pathways for oil migration should also be noticed. It found that a large number of natural fractures existed in continental shale, combining with the previous researches (Zhu, 2013; Ding et al., 2024) and the structure images in this study, it found that the natural cracks that mainly developed inside the dark lamination and at the interface positions of different laminations are the bedding cracks and the interface cracks, which affects both its mechanical property and the propagation path of new cracks (Fig. 8). Ju et al. (2022) summed up the crack propagation patterns when approaching the interface of a composite material (material A and material B) (Fig. 10(a)), and mentioned that the strength or toughness of interface, the geometrical properties of interface, and the dissimilar elastic properties of composite materials have significant influences on the crack propagation. In this study, the natural cracks have two states of full fill and incomplete fill, which affects the strength of fracture interface. With the increase in filling degrees, the bonding strength ratio between natural cracks and nascent cracks becomes larger due to the greater fracture energy required by the fracture filling materials (Sharafisafa et al., 2021), and the propagation patterns shift from deflection to direct penetration, which means that the deflection pattern easily appears in un-filled crack and the penetration pattern occurs in full-filled crack (Fig. 10(b)). Moreover, the morphology of natural cracks is consistent with the laminations, showing a wavy shape or oblique straight shape, which affects the geometrical property of the interface (such as interface angle). Thus, there is a transition of cracking patterns with changing of crack morphologies, which means that the deflection pattern is prone to occur in incline natural cracks and the penetration pattern is prone to occur at horizontal natural cracks (Zhang et al., 2022c; Cui and Hou, 2024) (Fig. 10(c)). In addition, some natural cracks occur at the boundary between muddy lamination and sandy lamination, which makes the dissimilar elastic properties of the composite materials. Research results (Buyukozturk and Hearing, 1998; Gudmundsson et al., 2010; Ju et al., 2022) shown that cracks are more likely to penetrate from the harder part into the softer part as well as from the part with high fracture toughness into the part with low fracture toughness. Thus, the strength and fracture toughness of sandy lamination are higher than those of muddy lamination in this study, then the combination relationship of laminations changes the crack propagation pattern, which means that the deflection pattern is likely to develop if crack propagating from muddy lamination to sandy lamination and the penetration pattern is likely to occur if crack propagating from sandy lamination to muddy lamination (Fig. 10(d)). Therefore, the relationship between the new and natural fractures of continental shale in true triaxial loading test can be mainly concluded as follows: direct penetration (vertical and incline) and deflection (single and double). In summary, the effect of interface cracks on the growth of new fractures is related to its own properties, such as filling degree, morphological characteristics, and the relationship of two side laminations, which is different from that of bedding in layered rocks.

5.3. Comprehensive evaluation of fracability

In addition to the mechanical parameters, Yuan et al. (2017), Meng et al. (2021), and Liu et al. (2023a) proposed that the influence of rock structure and in-situ stress should also be paid attention to. The laminar continental shale studied in this study has different structural characteristics from the marine and intercalated continental shale, and the structural heterogeneity resulted from the different types of laminations and interface cracks. The results of uniaxial compression tests of laminations and true triaxial compression tests of continental shale show that: (1) The difference of B_{rit} of laminations affects the type of new fractures, tensile fracture with larger opening formed in brittle sandy lamination and shear fractures with complex morphology formed in plastic muddy lamination. It can be seen that the conclusion that the higher B_{rit}, the easier it is to create a complex fracture network (Jin et al., 2015; Wang et al., 2020) is not suitable for a single lamination type. But for the whole lamination specimen, the

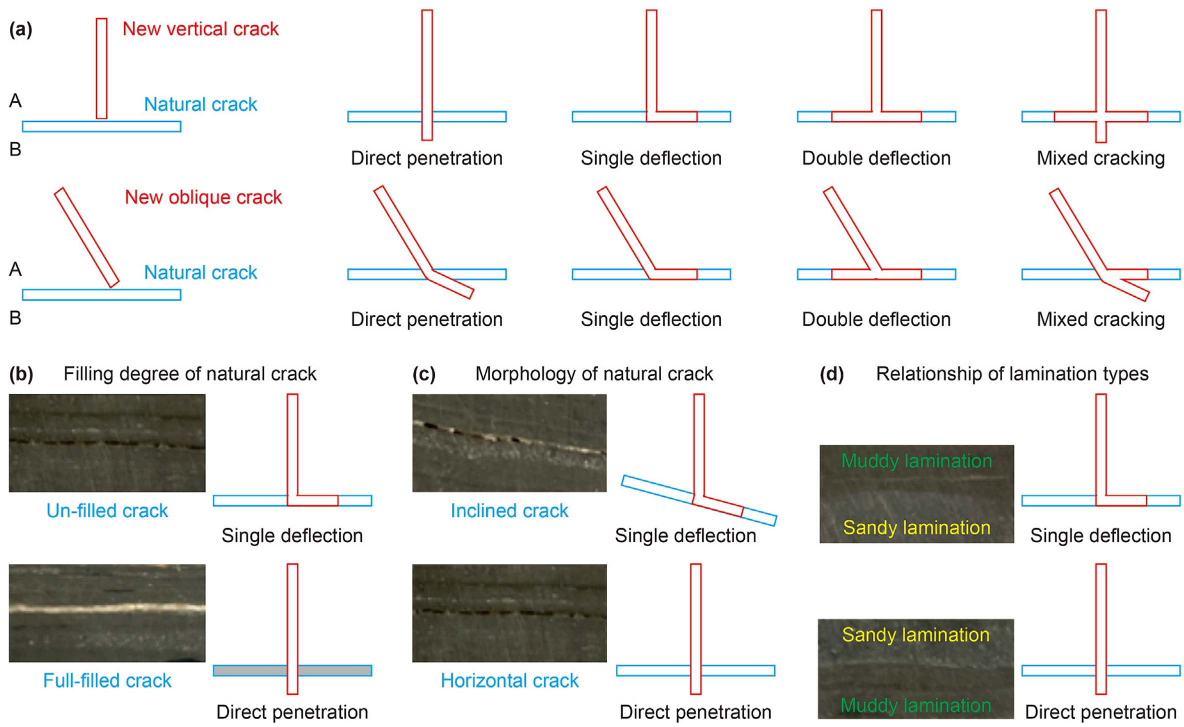

Fig. 10. Schematic diagram of crack propagation patterns when approaching the interface of composite material (**a**) (modified after Ju et al. (2022)) and the cracking patterns in this study affected by the filling degree (**b**), morphology (**c**) of natural cracks, and the relationship of laminations (**d**). (Note: (b), (c) and (d) take the vertical crack as an example, and the same six patterns also exist for an oblique crack).

composite fracture network of tensile and shear cracks is formed and the fracability is better. Therefore, the B_{rit} is still an indispensable index in evaluating the fracability of laminar continental shale, and the lamination combination should be considered. (2) The difference of K_c affects the number of new fractures, the K_{Ic} and K_{IIc} of muddy lamination are both smaller and more secondary cracks are formed inside it. This is followed in the conclusion that the lower K_c , the easier it is for the fracture to propagate (Yuan et al., 2017; Gupta et al., 2020). Therefore, the K_c is the second core index in evaluating the fracability of laminar continental shale. (3) The difference of filling degree and morphology of interface cracks control the communication mode between nascent fractures and natural fractures, and these mechanical properties of natural fractures (strength c_j and φ_j and fracture toughness K_{cj}) also contribute to the formation of complex fracture networks to a certain extent, which is consistent with the research result that with the increase in the number of the fracture density, the reservoir brittleness increased significantly (Liu et al., 2023b). Therefore, the B_{rit} and K_c of interface cracks are also important indexes when evaluating the fracability of laminar continental shale. The above three aspects are related to the shale structures and their mechanical properties, so the contribution of different types of laminations and interface cracks should be considered, respectively. That is, different from the previous studies, when considering the B_{rit} and K_c, the structural heterogeneity index H caused by the lamination combination and interface cracks distribution should be considered, such as the thickness ratios of different types of laminations and the spacing between interface cracks. (4) A complex fracture network is formed in the continental shale under a suitable horizontal stress difference ($\Delta\sigma_h = 5$–10 MPa) in this study, indicating that the influence of the horizontal in-situ stress difference that is different from the concept of the gradient of the minimum in-situ stress (Yuan et al., 2017) cannot be ignored. Therefore, the in-situ stress index S (the difference between the maximum horizontal principal stress and the minimum horizontal principal stress) must also be considered when evaluating the fracability of laminar continental shale.

To sum up, according to the results of previous studies and this study, for the comprehensive evaluation of fracability of laminar continental shale, in addition to considering the indexes of B_{rit} and K_c of different laminations and interface cracks, the structural heterogeneity index H caused by their geometric distribution and the in-situ stress index $\Delta\sigma_h$ should also be paid attention to. And the weights of those evaluation indexes can be determined and integrated into a system based on the analytic hierarchy process (Chen et al., 2024b), the entropy weight method (Huang, 2022) and the grey relation analysis (Xiong et al., 2023). In this study, the mechanical properties of laminations and their influences on crack propagation are revealed through laboratory rock mechanics tests. The relevant research tests, analysis methods and conclusions, especially that considering the characteristics of reservoir structure and their effects on reservoir fracability evaluation, can provide references for applications in other geological settings and depositional environments. However, the laboratory rock tests also have certain limitations, such as limited combination relationship of laminations and combination relationship of the loading stress conditions of the test samples. In order to overcome these limitations and validate, the simulation and theoretical analyses are considered to establish more numerical models of laminations property combinations and carry out more numerical studies under true triaxial loading stress conditions in the future to improve and develop the knowledge obtained from the existing laboratory tests.

6. Conclusions

Laminar continental shale is a favorable rock facies for shale oil enrichment, and the reservoir rock is with high heterogeneous. Identifying the mechanical characteristics of laminations of continental shale and the fracture mechanism under true triaxial loading can provide a theoretical basis for the proposal of indicators and methods for fracability evaluation. In this study, methods of multi-scale observation, XRD and thin slice analysis were used to define the lamination types of continental shale, and the real-time micro-CT uniaxial compression tests were carried out to obtain the mechanical parameters and failure characteristics of different laminations. On this basis, the true triaxial loading and CT scanning tests of continental shale were carried out to research the influence of mechanical parameters of laminations on fracture propagation of laminar continental shale, analyse the controlling mechanism of laminations and interface cracks characteristics on the growth of nascent fractures, and elucidate the structural control mechanism of laminar continental shale fracture. The main conclusions are as follows:

(1) Laminations of Chang 7_2 continental shale include the bright lamination and dark lamination in terms of the colour differences, as for the mineral composition and structure, the bright lamination has a high content of brittle minerals, such as quartz, forming a void structure, and the dark lamination has a high content of clay minerals, forming a layer structure. In view of this, combining the three aspects, two types of laminations are divided into the void-type sandy lamination and the layer-type muddy lamination.
(2) The uniaxial compressive strength and elastic modulus of sandy lamination specimen are higher, the Poission's ratio is smaller and the lateral deformation is not obvious, and simple crack with large opening is formed when it is broken. The values of uniaxial compressive strength and elastic modulus of muddy lamination specimen are smaller, Poisson's ratio is larger and the lateral deformation is more obvious, and secondary cracks between layers are more complex when the specimen is broken.
(3) Under the horizontal geo-stress difference condition of Chang 7 reservoir (5 and 10 MPa), the new fractures communicate the sandy lamination, muddy lamination, and interface cracks. Single vertical fracture is formed in sandy lamination, and a large number of oblique fractures are formed in muddy lamination. The structure combination of different laminations and natural cracks is conducive to forming complex fracture networks, indicating that the laminar continental shale is a favorable fracturing rock facies.
(4) Lamination types control the formation type and the number of new fractures: tensile crack formed in sandy lamination with higher brittleness index and shear cracks formed in plastic muddy lamination because of their deformation dissonance, and more secondary cracks developed in muddy lamination due to the smaller fracture toughness. Moreover, the characteristics (filling degree, morphology, and laminations relationship) of interface cracks also control the cracks propagation pattern: penetration and deflection.

CRediT authorship contribution statement

Yong-Ting Duan: Writing – original draft, Supervision, Project administration, Methodology, Investigation. **Cheng-Cheng Zhu:** Writing – review & editing, Methodology, Data curation. **Pathegama Gamage Ranjith:** Writing – review & editing. **Bai-Cun Yang:** Writing – review & editing, Methodology, Funding acquisition, Data curation. **Tian-Qiao Mao:** Software, Data curation. **Yu Li:** Methodology, Data curation.

Declaration of competing interest

The authors declare that they have no known competing financial interests or personal relationships that could have appeared to influence the work reported in this paper.

Acknowledgments

The authors thank the Editor and the anonymous reviewer for their helpful and constructive comments. This work was funded by the National Natural Science Foundation of China (42102309 and 42007243), the Natural Science Foundation of Liaoning Province (2023-MSBA-120), and the National Key Research and Development Program (2022YFB3304705).

References

Bao, S.J., Ge, M.N., Xu, X.Y., et al., 2023. Progress and development proposals in the exploration and development of continental shale oil in China. Chin. Geol. 50 (5), 1343–1354. https://doi.org/10.12029/gc20230105002. (in Chinese).
Bian, C.S., Guo, B.C., Pu, X.G., et al., 2023. Lithofacies characteristics and their effects on shale oil enrichment: A case study from Shahejie Formation of the Qibei Sag, Bohai Bay Basin, China. Energies 16 (5), 2107. https://doi.org/10.3390/en16052107.
Buyukozturk, O., Hearing, B., 1998. Crack propagation in concrete composites influenced by interface fracture parameters. Int. J. Solid Struct. 35 (31–32), 4055–4066. https://doi.org/10.1016/S0020-7683(97)00300-4.
Chandler, M.R., Meredith, P.G., Brantut, N., et al., 2016. Fracture toughness anisotropy in shale. J. Geophys. Res. Solid Earth 121 (3), 1706–1729. https://doi.org/10.1002/2015JB012756.
Chen, K., Duan, Y.W., Yu, X.M., et al., 2024b. Fracturability evaluation on sand-shale interbedded reservoir at forefront of Qingzi margin in Songnan basin. Well Test. 33 (4), 66–72. https://link.cnki.net/doi/10.19680/j.cnki.1004-4388.2024.04.011 (in Chinese).
Chen, K.Z., Zhou, W.J., Pan, Y.G., et al., 2023. Characterization of true triaxial rock bursts in sandstones with different water contents. Front. Earth Sci. 10, 1087849. https://doi.org/10.3389/feart.2022.1087849.
Chen, S., Wang, X.J., Li, X.Y., et al., 2024a. Geophysical prediction technology for sweet spots of continental shale oil: A case study of the Lianggaoshan Formation, Sichuan Basin, China. Fuel 365, 131146. https://doi.org/10.1016/j.fuel.2024.131146.
Cheng, S.Z., Sheng, M., Deng, C., 2024. Identification of different lithofacies laminations in oil shale and their mechanical properties. Front. Energy Res. 11, 1321853. https://doi.org/10.3389/fenrg.2023.1321853.
Cui, Z., Hou, B., 2024. Mechanical behavior of mixed-mode I-II fracture in deep laminated shale based on finite discrete element method. Theor. Appl. Fract. Mech. 133, 104596. https://doi.org/10.1016/j.tafmec.2024.104596.
Ding, W.L., Wang, Y., Wang, S.H., et al., 2024. Research progress and insight on nontectonic fractures in shale reservoirs. Earth Sci. Front. 31 (1), 297–314. https://link.cnki.net/doi/10.13745/j.esf.sf.2023.12.5 (in Chinese).
Duan, Y.T., Yang, B.C., 2022. How does structure affect the evolution of cracking and the failure mode of anisotropic shale? Geomechanics and Geophysics for Geo-Energy and Geo-Resources 8, 25. https://doi.org/10.1007/s40948-021-00330-w.
Duan, Y.T., Li, X., Zheng, B., et al., 2019. Cracking evolution and failure characteristics of Longmaxi Shale under uniaxial compression using real-time computed tomography scanning. Rock Mech. Rock Eng. 52, 3003–3015. https://doi.org/10.1007/s00603-019-01765-0.
Duan, Y.T., Li, X., Ranjith, P.G., et al., 2020. An investigation of the evolution of the internal structures and failure modes of Longmaxi Shale using novel X-ray microscopy. J. Petrol. Sci. Eng. 184, 106479. https://doi.org/10.1016/j.petrol.2019.106479.
Duan, Y.T., Feng, X.T., Li, X., et al., 2022a. Mesoscopic damage mechanism and a constitutive model of shale using in-situ X-ray CT device. Eng. Fract. Mech. 269, 108576. https://doi.org/10.1016/j.engfracmech.2022.108576.
Duan, Y.T., Feng, X.T., Li, X., et al., 2022b. Investigation of the effect of initial structure and loading condition on the deformation, strength, and failure characteristics of continental shale. Geomechanics and Geophysics for Geo-Energy and Geo-Resources 8 (6), 207. https://doi.org/10.1007/s40948-022-00521-z.
Duan, Y.T., Zhu, C.C., Yang, B.C., et al., 2024. Fracture propagation and failure mode characteristics of lamellar lacustrine shale under true triaxial compression conditions. Environ. Earth Sci. 83, 96. https://doi.org/10.1007/s12665-023-11390-4.
Fan, L.F., Fan, Y.D., Xi, Y., et al., 2022. Spatial failure mode analysis of frozen sandstone under uniaxial compression based on CT technology. Rock Mech. Rock Eng. 55, 4123–4138. https://doi.org/10.1007/s00603-022-02859-y.
Fan, L.F., Qiu, B., Gao, J.W., et al., 2023. A real-time visual investigation on microscopic progressive fatigue deterioration of granite under cyclic loading. Rock Mech. Rock Eng. 56, 5133–5147. https://doi.org/10.1007/s00603-023-03326-y.
Feng, X.T., Yang, C.X., 2023. Hard Rock Mechanics in Deep Engineering. Science

Press, Beijing, pp. 234–236.
Feng, X.T., Kong, R., Zhang, X.W., et al., 2019. Experimental study of failure differences in hard rock under true triaxial compression. Rock Mech. Rock Eng. 52, 2109–2122. https://doi.org/10.1007/s00603-018-1700-1.
Feng, X.T., Kong, R., Yang, C.X., et al., 2020. A three-dimensional failure criterion for hard rocks under true triaxial compression. Rock Mech. Rock Eng. 53, 103–111. https://doi.org/10.1007/s00603-019-01903-8.
Fu, J.H., Li, S.X., Niu, X.B., et al., 2020. Geological characteristics and exploration of shale oil in Chang 7 member of triassic Yanchang Formation, Ordos Basin, NW China. Petrol. Explor. Dev. 47 (5), 931–945. https://doi.org/10.1016/S1876-3804(20)60107-0.
Gao, J.W., Xi, Y., Fan, L.F., et al., 2021. Real-time visual analysis of the microcracking behavior of thermally damaged granite under uniaxial loading. Rock Mech. Rock Eng. 54, 6549–6564. https://doi.org/10.1007/s00603-021-02639-0.
Gao, Z.L., Liu, Z.B., Tian, F., et al., 2022. Strength, energy evolution and cracking process of sandstone under high-temperature and high-pressure coupled true triaxial compression. Geomechanics and Geophysics for Geo-Energy and Geo-Resources 8, 176. https://doi.org/10.1007/s40948-022-00490-3.
Gu, Y., Xu, S., Fang, C., et al., 2021. Brittleness evaluation of the Lower Silurian marine shale reservoirs: A case study of Longmaxi shale in Fenggang block, southern China. Interpretation 9 (2), T463–T474. https://doi.org/10.1190/INT-2020-0142.1.
Gudmundsson, A., Simmenes, T.H., Larsen, B., et al., 2010. Effects of internal structure and local stresses on fracture propagation, deflection, and arrest in fault zones. J. Struct. Geol. 32 (11), 1643–1655. https://doi.org/10.1016/j.jsg.2009.08.013.
Guo, X.S., Li, M.W., Zhao, M.Y., 2023. Shale oil development and utilization and its role in energy industry. Bull. Chin. Acad. Sci. 38 (1), 38–47. https://link.cnki.net/doi/10.16418/j.issn.1000-3045.20221027001 (in Chinese).
Gupta, I., Sondergeld, C., Rai, C., 2020. Fracture toughness in shales using nano-indentation. J. Petrol. Sci. Eng. 191, 107222. https://doi.org/10.1016/j.petrol.2020.107222.
He, J.H., Li, Y., Deng, H.C., et al., 2022. Quantitative evaluation and influencing factors analysis of the brittleness of deep shale reservoir based on multiple rock mechanics experiments. Journal of Natural Gas Geoscience 7 (5), 295–307. https://doi.org/10.1016/j.jnggs.2022.10.001.
Hu, S.Y., Zhao, W.Z., Hou, L.H., et al., 2020. Development potential and technical strategy of continental shale oil in China. Petrol. Explor. Dev. 47 (4), 877–887. https://doi.org/10.1016/S1876-3804(20)60103-3.
Huang, B.X., Li, L.H., Tan, Y.F., et al., 2020. Investigating the meso-mechanical anisotropy and fracture surface roughness of continental shale. J. Geophys. Res. Solid Earth 125 (8), e2019JB017828. https://doi.org/10.1029/2019JB017828.
Huang, C., Yang, C., Shen, F., 2019. Fracability evaluation of lacustrine shale by integrating brittleness and fracture toughness. Interpretation 7 (2), T363–T372. https://doi.org/10.1190/INT-2017-0110.1.
Huang, S., 2022. Compressibility evaluation of tight sandstone reservoir in S area. Northeast Petroleum University, 2022. https://link.cnki.net/doi/10.26995/d.cnki.gdqsc.2022.000099 (in Chinese).
Jia, C.Z., 2024. Prospects and five future theoretical and technical challenges of the upstream petroleum industry in China. Acta Pet. Sin. 45 (1), 1–14. https://doi.org/10.7623/syxb202401001. (in Chinese).
Jiang, J.Q., Feng, X.T., Yang, C.X., et al., 2021. Experimental study on the failure characteristics of granite subjected to weak dynamic disturbance under different σ_3 conditions. Rock Mech. Rock Eng. 54, 5577–5590. https://doi.org/10.1007/s00603-021-02542-8.
Jiao, F.Z., 2021. Theoretical technologies and practices concerning "volume development" of low pressure continental shale oil: Case study of shale oil in Chang 7 member, Ordos Basin, China. Nat. Gas Geosci. 32 (6), 836–844. https://doi.org/10.11764/j.issn.1672-1926.2021.02.012. (in Chinese).
Jin, X.C., Shah, S.N., Roegiers, J.C., et al., 2015. Fracability evaluation in shale reservoirs—An integrated petrophysics and geomechanics approach. In: SPE Hydraulic Fracturing Technology Conference. https://doi.org/10.2118/168589-MS.
Jin, Z.J., Zhu, R.K., Liang, X.P., et al., 2021. Several issues worthy of attention in current lacustrine shale oil exploration and development. Petrol. Explor. Dev. 48 (6), 1471–1484. https://doi.org/10.1016/S1876-3804(21)60303-8.
Ju, M.H., Li, X.F., Li, X., et al., 2022. A review of the effects of weak interfaces on crack propagation in rock: from phenomenon to mechanism. Eng. Fract. Mech. 263, 108297. https://doi.org/10.1016/j.engfracmech.2022.108297.
Kachanov, L.M., 1958. Time of the rupture process under creep conditions. Izvestiia Akademii Nauk SSSR, Otdelenie Teckhnicheskikh Nauk 8, 26–31.
Kong, R., Feng, X.T., Zhang, X.W., et al., 2018. Study on crack initiation and damage stress in sandstone under true triaxial compression. Int. J. Rock Mech. Min. Sci. 106, 117–123. https://doi.org/10.1016/j.ijrmms.2018.04.019.
Li, C.B., Xie, H.P., Wang, J., 2020. Anisotropic characteristics of crack initiation and crack damage thresholds for shale. Int. J. Rock Mech. Min. Sci. 126, 104178. https://doi.org/10.1016/j.ijrmms.2019.104178.
Li, L.H., Huang, B.X., Li, Y.Y., et al., 2019b. Multi-scale 3-D modeling of Yanchang shale geological structure considering laminas and fracture networks. J. Eng. Geol. 27 (1), 69–79. https://link.cnki.net/doi/10.13544/j.cnki.jeg.2019-061 (in Chinese).
Li, L.H., Huang, B.X., Li, Y.Y., et al., 2018. Multi-scale modeling of shale laminas and fracture networks in the Yanchang formation, Southern Ordos Basin, China. Eng. Geol. 243, 231–240. https://doi.org/10.1016/j.enggeo.2018.07.010.
Li, L.H., Huang, B.X., Tan, Y.F., et al., 2022b. Using micro-indentation to determine the elastic modulus of shale laminae and its implication: Cross-scale correlation of elastic modulus of mineral and rock. Mar. Petrol. Geol. 143, 105740. https://doi.org/10.1016/j.marpetgeo.2022.105740.
Li, M.Y., Chen, X.K., 2021. A comparison of geological characteristics of the main continental shale oil in China and the U.S. Lithosphere 2021, 3377705. https://doi.org/10.2113/2021/3377705.
Li, S.B., Liang, K., Wang, C.H., et al., 2022c. Study of wellbore instability and collapse mechanism for a layered continental shale oil horizontal well. Energies 15 (13), 4538. https://doi.org/10.3390/en15134538.
Li, S.X., Guo, Q.H., Zhou, X.P., et al., 2022a. Reservoir characteristics and exploration direction of pure shale-type shale oil in the 3rd sub member, 7th Member of Yanchang Formation in Ordos Basin. Acta Pet. Sin. 43 (11), 1509–1519. https://doi.org/10.7623/syxb202211001 (in Chinese).
Li, X., He, J.M., Yin, C., et al., 2019a. Characteristics of the shale bedding planes and their control on hydraulic fracturing. Oil Gas Geol. 40 (3), 653–660. https://doi.org/10.11743/ogg20190320 (in Chinese).
Li, Y., Xue, L., Wu, X.W., 2019c. Study on acoustic emission and X-ray computed-tomography characteristics of shale samples under uniaxial compression tests. Environ. Earth Sci. 78, 173. https://doi.org/10.1007/s12665-019-8185-4.
Lin, C., He, J.M., Liu, Y.D., et al., 2022. Quantitative characterization of cracking process in oil shale using micro-CT imaging. Arabian J. Geosci. 15, 301. https://doi.org/10.1007/s12517-021-09405-0.
Liu, B., Jin, L., Hu, C.Z., 2019. Fractal characterization of silty beds/laminae and its implications for the prediction of shale oil reservoir in Qingshankou Formation of northern Songliao Basin, Northeast China. Fractals 27 (1), 1940009. https://doi.org/10.1142/S0218348X19400097.
Liu, B., Wang, S., Ke, X., et al., 2020a. Mechanical characteristics and factors controlling brittleness of organic-rich continental shales. J. Petrol. Sci. Eng. 194, 107464. https://doi.org/10.1016/j.petrol.2020.107464.
Liu, K.Q., Ostadhassan, M., Bubach, B., 2016. Applications of nano-indentation methods to estimate nanoscale mechanical properties of shale reservoir rocks. J. Nat. Gas Sci. Eng. 35, 1310–1319. https://doi.org/10.1016/j.jngse.2016.09.068.
Liu, X.F., Feng, X.T., Zhou, Y.Y., 2020b. Experimental study of mechanical behavior of gneiss considering the orientation of schistosity under true triaxial compression. Int. J. GeoMech. 20 (11), 04020199. https://doi.org/10.1061/(ASCE)GM.1943-5622.0001838.
Liu, X.F., Feng, X.T., Zhou, Y.Y., 2023a. Influences of schistosity structure and differential stress on failure and strength behaviors of an anisotropic foliated rock under true triaxial compression. Rock Mech. Rock Eng. 56, 1273–1287. https://doi.org/10.1007/s00603-022-03133-x.
Liu, X.Y., Li, S.X., Guo, Q.H., et al., 2021. Characteristics of rock types and exploration significance of the shale strata in the Chang 7_3 sub-member of Yanchang Formation, Ordos Basin, China. Journal of Natural Gas Geoscience 6 (6), 363–373. https://doi.org/10.1016/j.jnggs.2021.12.003.
Liu, Y.J., Lai, F.Q., Wang, R.Y., et al., 2023b. Influencing factors of the brittleness of continental shales containing shell limestone interlayer. Minerals 13 (4), 460. https://doi.org/10.3390/min13040460.
Lu, J., Huang, G., Gao, H., et al., 2020. Mechanical properties of layered composite coal-rock subjected to true triaxial stress. Rock Mech. Rock Eng. 53 (9), 4117–4138. https://doi.org/10.1007/s00603-020-02148-6.
Lyu, Q.Q., Fu, J.H., Luo, S.S., et al., 2022. Sedimentary characteristics and model of gravity flow channel-lobe complex in a depression lake basin: A case study of Chang 7 Member of Triassic Yanchang Formation in southwestern Ordos Basin, NW China. Petrol. Explor. Dev. 49 (6), 1323–1338. https://doi.org/10.1016/S1876-3804(23)60352-0.
Ma, X., Dong, W.B., Hu, D.W., et al., 2023. Mechanical properties of granite at high temperature subjected to true triaxial compression. Int. J. Rock Mech. Min. Sci. 164, 105313. https://doi.org/10.1016/j.ijrmms.2022.105313.
Meng, S.W., Li, D.X., Wang, Q., et al., 2021. Nanoindentation-based three-parameter fracability evaluation method for continental shales. Front. Earth Sci. 9, 797405. https://doi.org/10.3389/feart.2021.797405.
Mi, S.J., Guo, Q.L., Zhang, Q., et al., 2023. Classification and potential of continental shale oil resources in China and resource evaluation methods and criteria. Oil Shale 40 (4), 283–320. https://doi.org/10.3176/oil.2023.4.02.
Ozcelik, Y., Kulaksiz, S., Cetin, M.C., 2002. Assessment of the wear of diamond beads in the cutting of different rock types by ridge regression. J. Mater. Process. Technol. 127 (3), 392–400. https://doi.org/10.1016/S0924-0136(02)00429-6.
Pu, B.L., Wang, F.Q., Zhao, W.W., et al., 2023. Identification and division of favorable intervals of the Chang 7 gas shale in the Yan'an area, Ordos Basin, China. Carbonates Evaporites 38 (4), 69. https://doi.org/10.1007/s13146-023-00890-w.
Qin, X.Y., Wang, Z.L., Yu, H.Y., et al., 2016. Geophysical well logging in brittleness evaluation based on rock mechanics characteristic—a case study from the member 7 shale of Yanchang Formation in southeast Ordos Basin. Prog. Geophys. 31 (2), 762–769 https://doi.org/10.6038/pg20160235. (in Chinese).
Rabotnov, Y.N., 1963. On the equations of state of creep. Proceedings of the Institution of Mechanical Engineers Conference Proceedings 178 (31), 117–122. https://doi.org/10.1243/PIME_CONF_1963_178_030_02.
Rickman, R., Mullen, M., Petre, E., et al., 2008. A practical use of shale petrophysics for stimulation design optimization: all shale plays are not clones of the barnett shale. In: SPE Annual Technical Conference and Exhibition. https://doi.org/10.2118/115258-MS.
Sharafisafa, M., Aliabadian, Z., Tahmasebinia, F., et al., 2021. A comparative study on the crack development in rock-like specimens containing unfilled and filled flaws. Eng. Fract. Mech. 241, 107405. https://doi.org/10.1016/

j.engfracmech.2020.107405.
Shi, H.L., Hosdez, J., Rougelot, T., et al., 2021. Analysis of local creep strain field and cracking process in claystone by X-ray micro-tomography and digital volume correlation. Rock Mech. Rock Eng. 54, 1937–1952. https://doi.org/10.1007/s00603-021-02375-5.
Shi, J.Y., Jin, Z.J., Liu, Q.Y., et al., 2022. Laminar characteristics of lacustrine organic-rich shales and their significance for shale reservoir formation: a case study of the Paleogene shales in the Dongying Sag, Bohai Bay Basin, China. J. Asian Earth Sci. 223, 104976. https://doi.org/10.1016/j.jseaes.2021.104976.
Sun, D.L., Liu, H., He, W.Y., et al., 2021. An analysis of major scientific problems and research paths of Gulong shale oil in Daqing Oilfield, NE China. Petrol. Explor. Dev. 48 (3), 527–540. https://doi.org/10.1016/S1876-3804(21)60043-5.
Sun, H.Q., Wang, H.T., Yang, Y., et al., 2024. Iteration and evaluation of shale oil development technology for continental rift lake basins. Petrol. Explor. Dev. 51 (4), 993–1008. https://doi.org/10.1016/S1876-3804(24)60520-3.
Sun, X.K., Li, X., Zheng, B., et al., 2020. Study on the progressive fracturing in soil and rock mixture under uniaxial compression conditions by CT scanning. Eng. Geol. 279, 105884. https://doi.org/10.1016/j.enggeo.2020.105884.
Wang, G.W., Chang, X.C., Yin, W., et al., 2017a. Impact of diagenesis on reservoir quality and heterogeneity of the Upper Triassic Chang 8 tight oil sandstones in the Zhenjing area, Ordos Basin, China. Mar. Petrol. Geol. 83, 84–96. https://doi.org/10.1016/j.marpetgeo.2017.03.008.
Wang, H.J., Liu, D.A., Huang, Z.Q., et al., 2017b. Mechanical properties and brittleness evaluation of layered shale rock. J. Eng. Geol. 25 (6), 1414–1423. https://link.cnki.net/doi/10.13544/j.cnki.jeg.2017.06.003 (in Chinese).
Wang, J.F., Yang, C., Liu, Y.K., et al., 2022a. Nanoindentation investigation of mechanical and creep properties of continental Triassic Yanchang Formation shale, Ordos Basin. Interpretation 10 (3), SJ29–SJ41. https://doi.org/10.1190/INT-2021-0218.1.
Wang, L., Guo, Y.T., Yang, C.H., et al., 2020. Mechanical characterization of continental shale in Sichuan Basin of China and its potential impact on reservoir stimulation. J. Nat. Gas Sci. Eng. 79, 103346. https://doi.org/10.1016/j.jngse.2020.103346.
Wang, X.J., Liang, L.X., Zhao, L., et al., 2019. Rock mechanics and fracability evaluation of the Lucaogou Formation oil shales in Jimusaer sag, Junggar Basin. Oil Gas Geol. 40 (3), 661–668. https://doi.org/10.11743/ogg20190321. (in Chinese).
Wang, X.Y., Gao, Q.C., Li, X., 2022b. Layer orientation effect on fracture mode and acoustic emission characteristics of continental shale. Appl. Sci. 12 (17), 8683. https://doi.org/10.3390/app12178683.
Woo, J., Lee, H.S., Ozyer, C., et al., 2021. Effect of lamination on shale reservoir properties: case study of the Montney Formation, Canada. Geofluids (1), 8853639. https://doi.org/10.1155/2021/8853639, 2021.
Wu, K., Meng, Q.S., Wang, C., et al., 2023. Experimental investigation of damage evolution characteristics of coral reef limestone based on acoustic emission and digital volume correlation techniques. Rock Mech. Rock Eng. 56, 2357–2374. https://doi.org/10.1007/s00603-022-03186-y.
Xi, K.L., Li, K., Cao, Y.C., et al., 2020. Laminae combination and shale oil enrichment patterns of Chang 7_3 sub-member organic-rich shales in the Triassic Yanchang Formation, Ordos Basin, NW China. Petrol. Explor. Dev. 47 (6), 1342–1353. https://doi.org/10.1016/S1876-3804(20)60142-8.
Xia, D.B., Yang, Z.M., Gao, T.N., et al., 2021. Characteristics of micro- and nano-pores in shale oil reservoirs. J. Pet. Explor. Prod. Technol. 11, 157–169. https://doi.org/10.1007/s13202-020-01012-1.
Xia, Y.J., Zhou, H., Zhang, C.Q., et al., 2022. The evaluation of rock brittleness and its application: A review study. European Journal of Environmental and Civil Engineering 26 (1), 239–279. https://doi.org/10.1080/19648189.2019.1655485.
Xia, Z.Y., Ma, H.Y., Fang, K., 2019. Rock mechanical properties and fracability of continental shale in zhanhua sag, Bohai Bay Basin. Petroleum Geology and Experiment 41 (1), 134–141. https://doi.org/10.11781/sysydz201901134 (in Chinese).
Xiong, J., Wu, J., Liu, X.J., et al., 2023. The geomechanical characteristics of the continental shale reservoirs and their influence on the fracturing effect. Journal of Southwest Petroleum University (Science & Technology Edition) 45 (5), 69–80. https://doi.org/10.11885/j.issn.1674-5086.2021.12.28.01. (in Chinese).
Xu, S., Gou, Q.Y., 2023. The importance of laminae for China lacustrine shale oil enrichment: a review. Energies 16 (4), 1661. https://doi.org/10.3390/en16041661.
Xue, L., 2015. A potential stress indicator for failure prediction of laboratory-scale rock samples. Arabian J. Geosci. 8, 3441–3449. https://doi.org/10.1007/s12517-014-1456-1.
Yang, H.Z., Wang, L., Yang, C.H., et al., 2023. Experimental investigation on different effects of fracturing fluids on mechanical properties and failure mechanism of continental shale. Int. J. Rock Mech. Min. Sci. 164, 105362. https://doi.org/10.1016/j.ijrmms.2023.105362.
Yang, L., Mao, Y.T., Yang, D., et al., 2022. The characteristic and distribution of shale micro-brittleness based on nanoindentation. Materials 15 (20), 7143. https://doi.org/10.3390/ma15207143.
Yang, R.C., Loon, A.J., Yin, W., et al., 2016. Soft-sediment deformation structures in cores from lacustrine slurry deposits of the Late Triassic Yanchang Fm. (central China). Geologoes 22 (3), 201–211. https://doi.org/10.1515/logos-2016-0021.
Yang, R.C., Fan, A.P., Han, Z.Z., et al., 2017. Lithofacies and origin of the late triassic muddy gravity-flow deposits in the Ordos Basin, central China. Mar. Petrol. Geol. 85, 194–219. https://doi.org/10.1016/j.marpetgeo.2017.05.005.
Yang, Z., Hou, L.H., Tao, S.Z., 2015. Formation conditions and "sweet spot" evaluation of tight oil and shale oil. Petrol. Explor. Dev. 42 (5), 555–565. https://doi.org/10.0000/1000-0747-42-555.
Yang, Z., Zou, C.N., Wu, S.T., 2019. Formation, distribution and resource potential of the "sweet areas (sections)" of continental shale oil in China. Mar. Petrol. Geol. 102, 48–60. https://doi.org/10.1016/j.marpetgeo.2018.11.049.
Yuan, H.Y., Cheng, Y.F., Li, Y.Z., 2015. Formation selection criteria for volume fracturing in Chang 7 tight reservoir in the Ordos Basin. Adv. Petrol. Explor. Dev. 10 (2), 67–71. https://doi.org/10.3968/7674.
Yuan, J.L., Zhou, J.L., Liu, S.J., et al., 2017. An improved fracbility-evaluation method for shale reservoirs based on new fracture toughness-prediction models. SPE J. 22 (5), 1704–1713. https://doi.org/10.2118/185963-PA.
Zhang, G.K., Li, H.B., Wang, M.Y., et al., 2020b. Crack initiation of granite under uniaxial compression tests: A comparison study. J. Rock Mech. Geotech. Eng. 12 (3), 656–666. https://doi.org/10.1016/j.jrmge.2019.07.014.
Zhang, J.N., Yu, H., Wang, Q., et al., 2022c. Hydraulic fracture propagation at weak interfaces between contrasting layers in shale using XFEM with energy-based criterion. J. Nat. Gas Sci. Eng. 101, 104502. https://doi.org/10.1016/j.jngse.2022.104502.
Zhang, Q.G., Wang, L.Z., Zhao, P.F., et al., 2022b. Mechanical properties of lamellar shale considering the effect of rock structure and hydration from macroscopic and microscopic points of view. Appl. Sci. 12 (3), 1026. https://doi.org/10.3390/app12031026.
Zhang, Q.X., Hou, B., Pang, H.W., et al., 2022a. A comparison of shale gas fracturing based on deep and shallow shale reservoirs in the United States and China. Comput. Model. Eng. Sci. 133 (3), 471–507. https://doi.org/10.32604/cmes.2022.020831.
Zhang, S.H., Wu, S.C., Zhang, G., 2020a. Strength and deformability of a low-porosity sandstone under true triaxial compression conditions. Int. J. Rock Mech. Min. Sci. 127, 104204. https://doi.org/10.1016/j.ijrmms.2019.104204.
Zhang, W., Liu, X.J., Liang, L.X., et al., 2024. Fracture characteristics of reservoirs with different lithologies in marine-continental transitional facies and its influence on fracturing. Petroleum Geology and Recovery Efficiency 31 (6), 1–15. https://link.cnki.net/doi/10.13673/j.pgre.202309029 (in Chinese).
Zhao, J.Z., Ren, L., Lin, C., et al., 2025. A review of deep and ultra-deep shale gas fracturing in China: status and directions. Renew. Sustain. Energy Rev. 209, 115111. https://doi.org/10.1016/j.rser.2024.115111.
Zhao, W.Z., Hu, S.Y., Hou, L.H., et al., 2020. Types and resource potential of continental shale oil in China and its boundary with tight oil. Petrol. Explor. Dev. 47 (1), 1–11. https://doi.org/10.1016/S1876-3804(20)60001-5.
Zhao, Z.H., 2018. Characteristics of Fracture Propagation Caused by Supercritical Carbon Dioxide and Hydraulic Fracturing in Shale. Doctoral Dissertation. Institution of Geology and Geophysics. Chinese Academy of Sciences, Beijing (in Chinese).
Zhou, W., Shi, G.X., Wang, J.B., et al., 2022. The Influence of bedding planes on tensile fracture propagation in shale and tight sandstone. Rock Mech. Rock Eng. 55, 1111–1124. https://doi.org/10.1007/s00603-021-02742-2.
Zhu, D.W., 2013. Developmental Characteristics, Major Regulating Factors and Distribution Prediction of Fractures in Shale of Upper Triassic Yangchang Formation in Yangchang Oil-Gas Field. Doctoral Dessertation. China University of Geosciences, Beijing (in Chinese).
Zou, C.N., Yang, Z., Li, G.X., et al., 2022. Why can China realize the continental "shale oil revolution". Journal of Earth Science 33 (5), 1324–1327. https://doi.org/10.1007/s12583-022-1745-7.